2 Phase Characteristics of Optical Filters

Christophe Peucheret

2.1 Introduction

Group velocity dispersion is a well known effect in optical fibres where the frequency dependence of the group index is responsible for pulse spreading, leading to inter-symbol interference (ISI) and power penalty [1]. However, it has only been realised recently that dispersive effects arising from optical filters might be detrimental to propagation of high bit-rate signals in wavelength division multiplexing (WDM) systems and networks [2, 3]. The need to take the dispersion of wavelength selective elements into account is being made more acute due to a number of technology trends. First, the increase of individual channel bit rates to 10 Gbit/s and the expected migration towards 40 Gbit/s per channel mean that even small dispersion values can no longer be ignored. Second, the quest for increased capacity in a single fibre has led to intense research in order to maximise the spectral efficiency and therefore reduce the channel spacing in WDM systems. Consequently, the relative bandwidth available to each channel is reduced, meaning that the channel experiences the effect of the edge of the passband of the filter transfer function, where the filter dispersion is expected to be most significant. Adjacent channel crosstalk reduction also triggers the need for WDM filters with steeper passband edges that, depending on the technology, are likely to result in increased dispersion [4, 5]. Finally, the evolution of WDM systems from point-to-point links to more complex network structures including optical add-drop multiplexers and optical cross-connects means that a number of filtering elements will be cascaded over the path of a specific channel. As the effect of dispersion is accumulative, more severe signal degradation is to be expected in future all-optical transparent networks [3, 6].

It has therefore become essential to be able to control the dispersion of optical WDM filters, either to limit potential signal degradation as in multiplexers and demultiplexers to be used in terminal equipment or within

add-drop and cross-connect nodes, or to provide tailorable dispersion as for example in chirped fibre Bragg gratings for dispersion compensation. The need for dispersion characterisation of optical filters has appeared in the mid-nineties, and suitable measurement methods have essentially been inspired from the experience gained in the characterisation of single mode optical fibres [7, 8]. However, specificities due the wavelength selective nature of the components often mean that known optical fibre characterisation solutions might not be directly transferred to the case of WDM filters. First, the desired bandpass or bandstop filter characteristics of most of the filters of interest will induce new requirements in terms of dynamic range of the measurement method, especially since the wavelength region where dispersion is expected to be significant corresponds to the edges of the transfer functions, where the attenuation of the device might be large. Second, WDM filters exhibit spectral features that are strongly wavelength dependent, as opposed to optical fibres where both attenuation and dispersion vary relatively slowly with wavelength. Finally, the dispersion values exhibited by WDM components are usually relatively small, whereas in the case of optical fibres the dispersion values to be measured can very often be made arbitrarily large by increasing the length of fibre over which the measurement is performed, assuming uniform distribution of the dispersion over the fibre length. The consequences of those new requirements on the choice of a suitable measurement method are discussed in more depth in this chapter. It should be noted that another branch of optics where similar challenges are met is the characterisation of components for femtosecond laser design, for which proper dispersion engineering is essential, owing to the short pulse widths involved [9].

This chapter gives a general introduction to the topic of phase-related characteristics of wavelength filters and further presents a number of techniques suitable for the characterisation of phase-related quantities (including group delay and dispersion) complemented by typical experimental results measured on relevant wavelength filters. Section 2.2 starts with a compilation of useful definitions and then focuses on causality arguments, which may be used to infer the phase response of some types of optical filters from their wavelength-dependent attenuation. A discussion of the applicability of the method is illustrated by a practical example. Two categories of techniques enabling the determination of dispersion-related quantities are presented in Sect. 2.3, namely interferometric methods and radio-frequency (RF) amplitude modulation techniques. Emphasis is given to low coherence interferometry and the modulation phase-shift methods as they are very often considered as the methods of choice for WDM filter characterisation. General dispersion properties of WDM filters are presented in Sect. 2.4 together with their consequences on optical communication system design.

Methods for evaluating the impact of WDM filter dispersion on the limitation of their usable bandwidth and cascadability are introduced. The effect of group delay ripples is also discussed. Finally, some examples of passband and dispersion engineering for the design of advanced WDM filters are provided. Properties specific to a given filter technology are described in more detail in the relevant chapters elsewhere in this book.

2.2 Theoretical Considerations

2.2.1 Definitions

Throughout this chapter the transfer function of an optical linear element, such as a wavelength filter, will be written

$$H(\omega) = \left|H(\omega)\right| e^{-i\phi(\omega)} . \tag{2.1}$$

Note that the definition of the sign of the phase in (2.1) might differ from the one used in some other chapters of this book. According to the theory of linear systems, the transfer function is the Fourier transform of the impulse response of the filter

$$H(\omega) = \int_{-\infty}^{+\infty} h(t)\, e^{-i\omega t} dt . \tag{2.2}$$

The group delay of the filter can be calculated from the phase of its transfer function according to

$$\tau = \frac{d\phi}{d\omega} . \tag{2.3}$$

The definition of τ is sometimes also found with negative sign (cf. e. g. Chaps. 8 and 9). This is a consequence of the choices of the sign for the phase in the definition of transfer functions such as (2.1), as well as of the time dependence in the complex representation of the electric field.

In practice, only the relative group delay is of practical interest as it is the variations of τ with wavelength that result in pulse distortion, therefore making it unnecessary to characterise the absolute group delay. The dispersion, usually expressed in ps/nm, is the derivative of the group delay with respect to wavelength

$$D = \frac{d\tau}{d\lambda} . \tag{2.4}$$

It can be checked that the set of definitions above is fully consistent with that customarily used for optical fibres, where D would represent the total dispersion accumulated over a length L of fibre.

2.2.2 Minimum-phase Filters and Amplitude-phase Relations

It is known from the theory of linear systems that the phase response of a filter can be inferred from its amplitude response provided the so-called "minimum-phase" condition is satisfied [10, 11]. It is therefore natural to consider such a numerical approach to retrieve the dispersion from the amplitude transfer function of optical filters. Provided the minimum-phase condition holds, the mathematical relations linking the amplitude and the phase of an optical filter are analogous to the Kramers–Kronig relations between the absorption and refractive index (or real and imaginary parts of the dielectric constant) of a material [12]. Mathematically, quantities satisfying such relations are known as Hilbert transform pairs. As a consequence, "amplitude-phase", "Kramers–Kronig", or "Hilbert transform" relations are often used indifferently in the context of wavelength filter characterisation. In this section, the conditions for the existence of such relations are presented, followed by a discussion of their practical use for the determination of the dispersive properties of WDM filters.

The Minimum-phase Condition

Let us consider a passive linear optical filter with impulse response $h(t)$. Such a physical system is causal and stable, therefore its impulse response is real valued and satisfies the conditions $h(t) = 0$ for $t < 0$ and $|h(t)| < \infty$. Let $H(\omega)$ be the transfer function of the optical filter (i. e. the Fourier transform of its impulse response) and $H_L(s)$, where s is a complex variable, its Laplace transform. The Fourier transform can be evaluated from the Laplace transform according to $H_L(i\omega) = H(\omega)$. The fact that $h(t)$ is causal translates into $H_L(s)$ being analytic in the right-hand plane. Under those assumptions it can be shown that

$$H(\omega) = \frac{1}{i\pi} P \int_{-\infty}^{+\infty} \frac{H(\Omega)}{\Omega - \omega} d\Omega \tag{2.5}$$

where P denotes the Cauchy principal value. Equation (2.5) can be derived either from causality considerations for the impulse response (see e. g. [13]) or, equivalently, from contour integration along a path where $H(\Omega)$ is analytic and avoiding the singularity at $\Omega = \omega$.

One important consequence of (2.5) is that the real (respectively imaginary) part of the transfer function $H(\omega)$ can be determined from the knowledge of its imaginary (respectively real) part. The real and imaginary parts of $H(\omega)$ are said to constitute a Hilbert transform pair.

The logarithm of the transfer function of a linear device as defined in (2.1) can be expressed as

$$\ln H(\omega) = \ln\left|H(\omega)\right| - i\phi(\omega). \tag{2.6}$$

Therefore, by applying the results of (2.5) to the function $\ln H(\omega)$, it is tempting to derive Hilbert transform relations between the logarithm of the amplitude transfer function and the phase of an optical filter. However, this would require the function $\ln H_L(s)$ to fulfil the initial assumption of being analytic in the right-hand plane. One important issue is that $H_L(s)$ might have zeros in the right-hand plane where the logarithm is not defined. If we moreover assume that $H_L(s)$ has no zeros for $\Re(s) \geq 0$, where $\Re$ denotes the real part, then its phase will be uniquely determined by its amplitude response according to

$$\phi(\omega) = \frac{1}{\pi} P \int_{-\infty}^{+\infty} \frac{\ln|H(\Omega)|}{\Omega - \omega}\, d\Omega\,. \tag{2.7}$$

Filters for which the logarithm of the Laplace transform of their impulse response is analytic in the right-hand plane are said to be of the "minimum-phase" type.

Amplitude-phase expressions that are equivalent to (2.7) are often found in the literature. For instance, starting from (2.7) and performing the change of variable $u = \ln \Omega/\omega$, a new expression for the phase can be written which highlights the relation between the variations of the amplitude response with frequency and the phase response

$$\phi(\omega) = \frac{1}{\pi} \int_{-\infty}^{+\infty} \frac{d}{du}\left[\ln|H(\omega e^{u})|\right] \ln\coth\frac{|u|}{2}\, du\,. \tag{2.8}$$

The factor $\ln\coth|u|/2$ peaks around $u = 0$ corresponding to $\Omega = \omega$ and exhibits a fast decrease when $|u|$ increases. Consequently, the main contribution to the integral (2.8) arises from values in the vicinity of $u = 0$, and the phase of the transfer function at ω depends mostly on the slope of the amplitude transfer function around the same frequency ω. An immediate consequence is that any attempt to realise sharp edges in the transfer function of a minimum-phase optical band-pass filter will result in increased dispersion at those edges. Recalling our discussion of Sect. 2.1, it can be concluded that, for a minimum-phase optical filter, the two goals of achieving low crosstalk and low dispersion cannot be reached simultaneously. Filters which are not minimum-phase will offer more degrees of freedom in order to achieve these two desired features. Note, however, that the fact that a filter is non minimum-phase does not prevent it from exhibiting a high dispersion at the edges of its passband, but simply means that its dispersion cannot be calculated from the attenuation spectrum.

Practical Applicability of Amplitude-phase Relations

Some early work on the applicability of the Kramers–Kronig relations to the determination of the group delay of optical filters was first presented in [14] in the context of sub-picosecond laser design at 800 nm, where it was clearly demonstrated that such relations do not necessarily exist for some types of filters. Their applicability to etalon filters was further discussed in [15] where the need for a careful consideration of the zeros of the transfer function as well as of the frequency dependence of all optical parameters was highlighted. At the same time, the determination of the dispersion of components to be used in WDM systems around 1550 nm became the object of increased attention. Kramers–Kronig relations were successfully applied to the reflectivity of fibre Bragg gratings (FBG) [16, 17], showing good agreement between recovered and theoretical group delay. A comparison between measured group delay and delay recovered from measured amplitude responses was later presented in [18] for uniform fibre gratings, showing good agreement for some devices. It was later on nevertheless suggested that, for real imperfect gratings, the modelling of the group delay of the corresponding perfect grating will often provide a better estimate than the recovery of the group delay by applying the Kramers–Kronig relations to the measured reflectivity [19].

The first step in determining the dispersive properties of a particular WDM filter based on Kramers–Kronig analysis is therefore to analyse whether this filter is of the minimum-phase type. An in-depth discussion of the applicability of the minimum-phase condition for different optical filter technologies has been presented in [5]. It was shown that generalised Mach–Zehnder filters (including arrayed waveguide gratings) are in general not minimum-phase. Interference filters such as Fabry–Perot and thin-film filters are inherently of the minimum-phase type when used in transmission. It has also been shown that grating filters are minimum-phase in transmission but that it is not always the case in reflection [20]. Nevertheless, in case the grating is symmetric, its group delay is identical in reflection and transmission, therefore enabling the reflection group delay to be recovered from the grating transmittivity.

Whether a given filter is of the minimum-phase type can in theory be determined from checking the analyticity of its transfer function in the right-hand plane provided the filter response can be accurately modelled. However, this does not necessarily imply that the real, imperfect, implementation of the filter belongs to the same category (minimum or non-minimum phase). Indeed, it has been reported that the effect of loss in arrayed waveguide grating filters can move the zeros of their complex transfer functions from the imaginary axis to the left-hand plane [5], making the real

filters satisfy the minimum-phase condition. Note that in the case when its zeros in the right-hand plane are known, a transfer function can be decomposed into the product of a minimum-phase function and an all-pass transfer function [15, 19] from which the phase response can be calculated. However, such an approach is not usable when the only information available about the filter is a measured amplitude response over a small part of the real frequency axis.

Once it has been ensured that the filter is minimum phase, practical considerations such as the frequency range over which the integration (2.7) needs to be performed as well as the implementation of the phase retrieval algorithm and its robustness to noisy measurement data and close to the zeros of the transfer function need to be taken into account. Numerous techniques have been proposed in the literature in order to compute Kramers–Kronig relations (see e. g. [21, 22] and the references in [23]). In the context of WDM filters, a calculation algorithm based on a non-linear frequency transformation known as the Wiener–Lee transform [10] has been applied to the case of fibre Bragg gratings [17] as well as a method using digital signal processing techniques [24]. More recently, an iterative approach [25] has shown its effectiveness at reconstructing the group delay of fibre gratings based on their transmission, even in the presence of significant noise.

As an illustration the amplitude-phase algorithm described in [17] has been applied to the case of a uniform fibre Bragg grating used in reflection. Such a symmetrical grating is known to be of the minimum-phase type [5, 20]. The measured reflectivity of a uniform fibre Bragg grating with

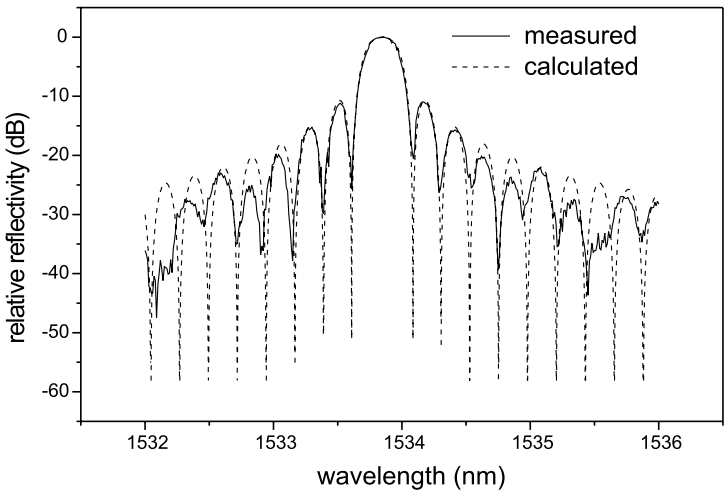

Fig. 2.1. Comparison of the measured and calculated power transfer functions in reflection for a 33 GHz uniform fibre Bragg grating

full-width half-maximum (FWHM) bandwidth equal to 33 GHz is plotted in Fig. 2.1 together with the corresponding theoretical transfer function calculated using the coupled mode equations formalism [26], showing good agreement for the main lobe and the first two sidelobes on both sides.

The phase responses calculated from the measured and theoretical reflectivities using the Wiener–Lee transform algorithm are shown in Fig. 2.2 (top). Good agreement is observed at the centre of the reflectivity main lobe. The phase discontinuities occur at the minima of the reflectivity where, due to imperfections in the real grating and the limited resolution of the optical spectrum analyser used for amplitude transfer function measurements, the measured and calculated reflectivities deviate significantly, hence the discrepancies observed for the phase.

The group delay calculated by differentiating the phase retrieved using the Wiener–Lee transform algorithm applied to the theoretical reflectivity and the theoretical group delay obtained using coupled mode equations are compared in Fig. 2.2 (bottom). Apart from the spikes in the recovered group delay occurring close to the zeros of the reflectivity, a good agreement is obtained, especially in the main lobe of the transfer function. Note that the theoretical group delay curve has been slightly up-shifted in Fig. 2.2 in order to allow for an easier comparison.

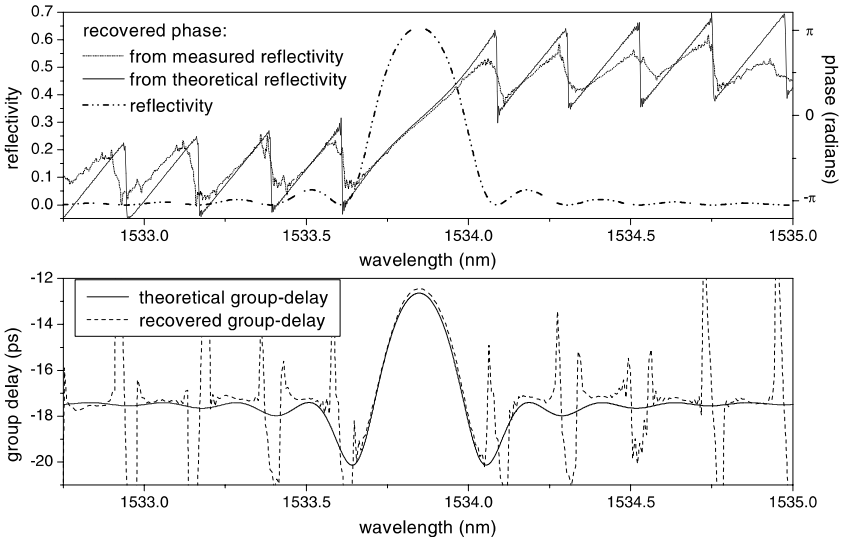

Fig. 2.2. (*Top*) phase responses calculated by applying the Wiener–Lee transform algorithm to the measured and calculated reflectivities of the uniform fibre grating whose transfer function is represented in Fig. 2.1. The calculated reflectivity is also plotted on a linear scale. (*Bottom*) corresponding theoretical group delay and group delay recovered from the theoretical reflectivity

The example above nevertheless confirms the concerns raised in [19] regarding the practical applicability of the method. Even if the main features of the phase or group delay of a filter that is known to be of the minimum-phase type can be retrieved by Kramers–Kronig analysis, the accuracy of the method might be questioned when it deals with the characterisation of the phase of imperfect real devices.

2.3 Measurement of the Dispersion of WDM Components

Due to the aforementioned difficulties associated with the use of amplitude-phase relations, direct measurement of the phase, group delay or dispersion of WDM filters is often preferred. In this section, two broad categories of phase-related quantities measurement techniques, based on either interferometry or small signal amplitude modulation of a continuous lightwave, are presented, and their advantages and limitations discussed.

2.3.1 Interferometric Techniques

A broad class of techniques enabling the characterisation of phase-related quantities makes use of interferometers where phase shifts can be converted into intensity variations that can be detected using a conventional photodiode. Several approaches have been followed in order to measure the phase properties of optical filters. A common difficulty to most implementations is the need for stabilisation schemes aimed at suppressing phase drifts as well as a precise calibration of the measurement set-up in the absence of the device under test.

Some early measurements have made use of coherent sources for the characterisation of the phase of optical filters. For instance in [27], measuring the power oscillations at the output of a Michelson interferometer while a laser was tuned over the device passband enabled to characterise the dispersion of a bulk grating pair as well as that of a linearly chirped waveguide grating. An all-fibre Michelson interferometer using phase modulation in the reference arm and lock-in detection was proposed in [28] and was used for some of the first characterisations of the group delay of a variety of fibre gratings [29]. The technique directly measures the phase change induced by the device under test while a laser is tuned over its passband. Phase-locked interferometry, where the delay of the reference arm of a Michelson interferometer is continuously adjusted while the wavelength is scanned, has been shown to enable group delay measurements with high temporal and spectral resolution, however at the

price of a complex experimental set-up where the delay is measured using the interference pattern of an auxiliary coherent source [30].

A second approach consists of a wavelength domain analysis of the interference fringes obtained at the output of a Michelson or Mach–Zehnder interferometer under broadband illumination. Initially applied to the characterisation of short lengths of optical fibres [31], the technique has also been used for the characterisation of wavelength-selective elements such as a grating pair [32] and, more recently, short lengths of photonic bandgap fibres [33]. Dispersion affects the wavelength periodicity of the interference fringes measured using an optical spectrum analyser. The local maxima or minima of the phase versus wavelength correspond to slow modulation of the interference fringes. Once the phase turning points have been identified, the phase can be fully reconstructed by keeping in mind that consecutive local maxima of the fringes on either side are obtained for phase jumps of $\pm 2\pi$. The interferometer needs to be balanced within the coherence length of the source, requiring a tuneable path length in the reference arm and possibly stabilisation of its operating point. Both temporal and spectral resolution depend on the number of interference fringes visible in the bandwidth of the device under test, making the method unsuitable for narrow filters with low dispersion. On the other hand, wide bandwidth and highly dispersive devices could be characterised by this technique as long as the knowledge of small group delay ripples is not required.

Low Coherence Interferometry

A powerful approach to the characterisation of the group delay of WDM filters is low coherence interferometry [34–36], also sometimes known as Fourier transform spectroscopy. A typical low coherence interferometry set-up is represented in Fig. 2.3 in a Mach–Zehnder configuration suitable for the characterisation of transmission filters such as arrayed waveguide gratings [37]. Reflective devices such as fibre Bragg gratings can be characterised in the same set-up using a circulator or in an equivalent Michelson interferometer configuration [38]. A low coherence source generates a broadband signal that is input to a 3 dB coupler. The device under test is inserted into one of the arms of the Mach–Zehnder interferometer while the second arm contains a variable length reference path. When the optical path length difference between the light contributions propagating in the two arms of the interferometer is within the coherence length of the source, interference fringes are obtained at the output 3 dB coupler and can be recorded via a photodetector followed by an analogue-to-digital converter for further processing.

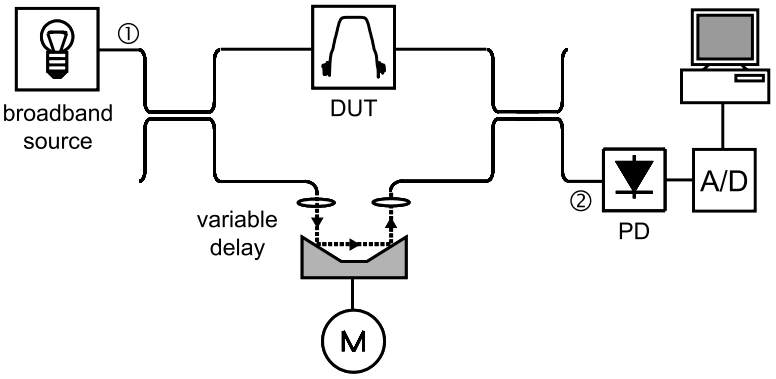

Fig. 2.3. Low coherence Mach–Zehnder interferometer for the measurement of the complex transfer function of optical filters used in transmission. An equivalent Michelson structure can be used for reflective devices. DUT: device under test; PD: photodiode; A/D: analogue-to-digital converter; M: motor driving the translation stage setting the variable delay

The method can be understood as follows. Let $E_1(t)$ and $E_2(t)$ be the contributions to the electric field at the output 3 dB coupler that have propagated from the source through the upper and lower arm of the interferometer, respectively. Let t_1 and t_2 be the delays from port ① to port ② corresponding to propagation through the device under test (DUT) and the reference arm, respectively. Let $E(t)$ be the field emitted by the source and $S(\omega)$ its spectral density. The intensity detected at port ② is proportional to the square of the modulus of the field averaged over a large number of optical cycles

$$I(t) = \left\langle \left| E_1(t) + E_2(t) \right|^2 \right\rangle, \tag{2.9}$$

where the angled brackets denote time averaging. Assuming identical polarisations for E_1 and E_2, the intensity becomes

$$I(t) = \left\langle E_1(t) E_1^*(t) \right\rangle + \left\langle E_2(t) E_2^*(t) \right\rangle + 2\Re\left\langle E_1(t) E_2^*(t) \right\rangle. \tag{2.10}$$

The first two terms are constant (dc) offsets, while the interference term can be shown to contain information about the transfer functions of the two arms of the interferometer. If the transfer functions of the device under test and of the reference path are denoted $H(\omega)$ and $H_{ref}(\omega)$, respectively, the two contributions to the total field at port ② can be written, assuming an ideal 3 dB coupler and neglecting the equal constant phase shifts experienced in the couplers along the two paths,

$$E_1(t) = \frac{1}{4\pi} \int_{-\infty}^{+\infty} \tilde{E}(\omega)\, H(\omega)\, e^{i\omega(t-t_1)}\, d\omega, \tag{2.11}$$

where $\tilde{E}(\omega)$ is the Fourier transform of the input field $E(t)$. In a similar way

$$E_2(t) = \frac{1}{4\pi} \int_{-\infty}^{+\infty} \tilde{E}(\omega)\, H_{ref}(\omega)\, e^{i\omega(t-t_2)}\, d\omega\,. \tag{2.12}$$

Hence the interference term

$$\left\langle E_1(t) E_2^*(t) \right\rangle = \left(\frac{1}{4\pi}\right)^2 \iint \left\langle \tilde{E}(\omega)\tilde{E}^*(\omega') \right\rangle H(\omega) H_{ref}^*(\omega') e^{i(\omega-\omega')t} e^{i(\omega' t_2 - \omega t_1)} d\omega d\omega' \tag{2.13}$$

With the usual assumptions of ergodicity and stationarity for the field $E(t)$, the time average can be replaced by ensemble average and it can be shown that

$$\left\langle \tilde{E}(\omega)\tilde{E}^*(\omega') \right\rangle = 2\pi\, \delta(\omega'-\omega) S(\omega) \tag{2.14}$$

where δ is the Dirac delta function. The interference term in (2.10) can therefore be written

$$I_{ac}(\tau_{21}) = 2\Re\left\langle E_1(t) E_2^*(t) \right\rangle = \frac{1}{2}\Re F^{-1}\left[S(\omega) H(\omega) H_{ref}^*(\omega)\right] \tag{2.15}$$

where F^{-1} denotes inverse Fourier transform. The argument of the interference term is the difference in time delay $\tau_{21} = t_2 - t_1$ that is linked to the optical path difference Δx between the light propagating in each of the arms of the interferometer. Consequently, if the interference fringes are recorded while Δx is changed by continuously increasing the length of the reference path along a translation stage, the interferogram $I(\Delta x)$ contains information about the complex transfer function (therefore including the desired phase information) of the device under test. In practice the Fourier transform of the fringes also contains information about other devices in the test path (such as the optical fibre patch cords, imperfections in the 3 dB coupler, etc.). However, performing a measurement scan without the device under test enables a total calibration of the set-up from which the parasitic contributions to the measured $H(\omega)$ as well as $H_{ref}^*(\omega)S(\omega)$ can be determined.

A variant of the technique makes use of a tuneable narrow band source and detects the shift of the centre of the fringes' envelope when the wavelength of the source is changed, enabling a direct determination of the variations of the group delay with wavelength [9, 34]. The time resolution depends on the visibility of the fringes' envelope which improves with increasing source bandwidth, while the spectral resolution is also obviously limited by the bandwidth of the source, making the method only suitable for the characterisation of broad bandwidth components. An all-fibre implementation of a low coherence reflectometry technique suitable for the characterisation of a broadband grating was also presented in [39].

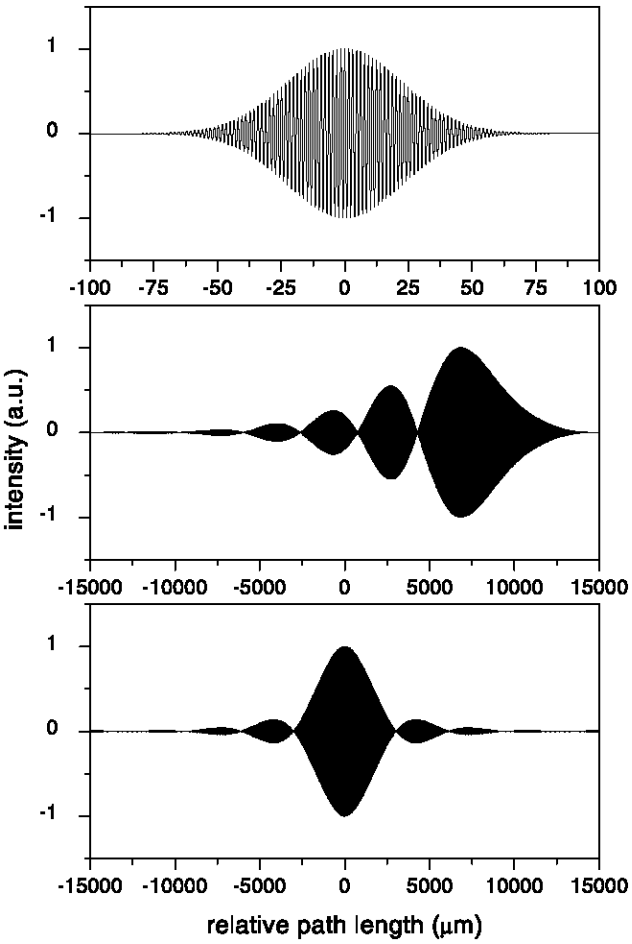

Fig. 2.4. Calculated low coherence interference fringes obtained from a broadband Gaussian source with 40 nm FWHM (*top*) and after reflection by a fibre Bragg grating filter designed for 50 GHz channel spacing (*centre*). Fourier transforming the fringes enables the determination of the spectral density of the source and the complex transfer function of the filter. Interference fringes that would be obtained from a linear phase grating with identical amplitude transfer function are also represented for comparison (*bottom*)

Figure 2.4 shows calculated low coherence interferometry fringes obtained by using a broadband source modelled as having a Gaussian spectrum with 40 nm full-width half-maximum (FWHM) bandwidth. The interferograms have been calculated with and without a Gaussian apodised grating designed for WDM systems with 50 GHz channel spacing in the test arm of the Michelson interferometer. Fourier transforming the interference fringes would enable to recover the grating complex transfer

function. In order to illustrate that the phase transfer function is indeed influencing the recorded interferogram, an additional calculation has been performed where a hypothetical device having the same amplitude response as the 50 GHz grating, but linear phase, was considered in the test arm of the interferometer. Note that the spatial spread of the interferograms is larger in the presence of the optical filter as a consequence of band limitation. Consequently the larger scale used in the centre and bottom graphs of Fig. 2.4 does not enable to resolve the interference fringes but only their envelope.

The method is fast since both, amplitude and phase characteristics of the filter, can be obtained with a single scan of the tuneable delay line. However, it requires a high linearity of the translation stage in the reference arm. In practice a second interferometer making use of e. g. an He-Ne laser is used to monitor the change in path length while the variable delay is scanned. The wavelength resolution depends on the scanning range and can be increased by zero padding the interferogram before applying a fast Fourier transform (FFT) algorithm. The technique has also been shown to exhibit a large dynamic range [38], making it suitable for the characterisation of the dispersion at the edges of the passband of WDM filters. However, the visibility of the fringes decreases when a bandpass element such as a WDM filter is included in the test arm. As the group delay and dispersion are obtained by differentiation of the phase, a sufficient signal-to-noise ratio should be ensured to avoid numerical errors. Smoothing of the measured data, averaging over multiple scans, or enhanced balanced detection can be applied.

The use of low coherence interferometry has been reported for the characterisation of fibre Bragg gratings [38, 40], showing clear benefits in terms of accuracy and acquisition speed compared to the widely used modulation phase-shift method that will be described in Sect. 2.3.2, however at the price of increased complexity of the measurement set-up. One unique feature of the method is the possibility to retrieve the group delay characteristics of individual gratings in a cascade, provided the contribution of each component to the interferogram can be isolated, or by processing of the entire interferogram if the reflection bands of the gratings do not overlap [41]. The method has also been successfully applied to the characterisation of the dispersion of arrayed waveguide gratings (AWGs). In one approach the entire interferogram is Fourier transformed, directly leading to the device dispersion [37]. Resolving the respective contributions of each waveguide in the array, from which the phase and amplitude error distribution can be determined, has also been shown to enable full accurate modelling of the AWG including its dispersion [37, 42, 43].

2.3.2 RF Modulation Methods

The Modulation Phase-shift Method

Due to its relative simplicity of implementation, the modulation phase-shift (MPS) technique [44, 45] has become the method of choice for characterisation of the dispersion of optical fibres as well as of optical components. Early reports of the use of the MPS method for WDM filters focused on devices such as Mach–Zehnder planar dispersion equalisers [46] or arrayed waveguide grating multiplexers [3]. A typical phase-shift set-up is shown in Fig. 2.5. Light from a continuous wave (CW) tuneable laser is externally modulated with a sinusoidal signal at frequency f_m using a Mach–Zehnder modulator (MZM). The choice of the modulation frequency, typically from a few tens of megahertz up to a few gigahertz, will be discussed in detail later. The modulated light is then input to the device under test before being detected by a photodiode. The photocurrent is bandpass filtered around f_m before being input to a vector voltmeter (VM). In practice, a network analyser can conveniently be used to provide the radio frequency signal used to drive the modulator and perform relative phase measurements. Comparison of the phase of the detected photocurrent at f_m with the reference phase of the modulating signal enables the determination of the group delay of the device under test according to

$$\Delta\varphi = 2\pi f_m \tau(\lambda_0) \tag{2.16}$$

where λ_0 is the wavelength of the tuneable laser source that is precisely monitored using a wavelength meter (WM). Repeating the measurement while the wavelength is tuned over the wavelength range of interest enables

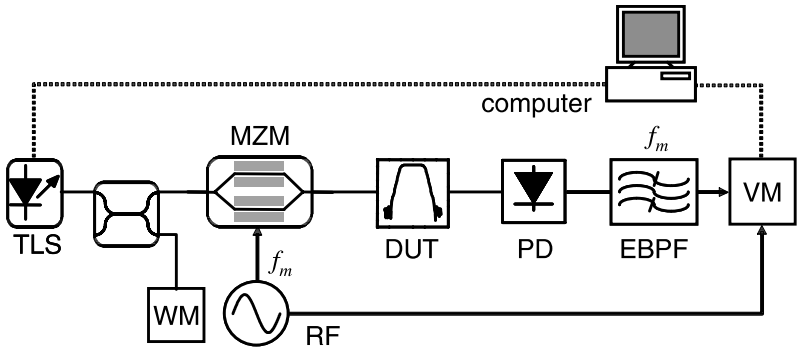

Fig. 2.5. Modulation phase-shift measurement set-up. TLS: tuneable laser source; WM: wavelength meter; MZM: Mach–Zehnder modulator; RF: radio frequency signal generator; DUT: device under test; PD: photodiode; EBPF: electrical bandpass filter; VM: vector voltmeter

the determination of the relative group delay as a function of wavelength from which the dispersion can theoretically be calculated according to (2.4).

In order to understand the limitations of the MPS method, it is essential to clarify the assumptions under which (2.16) has been derived. The complex representation of the electric field at the output of the MZM can be written

$$E_{in}(t) = E_0\left[1 + m\cos(\omega_m t - \varphi)\right]e^{i\omega_0 t} \tag{2.17}$$

where ω_0 is the angular frequency of the continuous lightwave generated in the tuneable laser, ω_m is the modulation angular frequency, φ is the phase of the modulating signal, and m is the modulation index. The spectrum of the modulated signal consists of a carrier at ω_0 and of two side-bands at $\omega_0 - \omega_m$ and $\omega_0 + \omega_m$. The electric field at the output of the DUT, whose complex transfer function has been defined according to (2.1), can easily be calculated by considering the attenuation and phase shifts experienced by the carrier and the two side-bands. If it is assumed that the carrier and the two side-bands experience the same amount of attenuation from the DUT (i. e. the magnitude of its transfer function can be considered constant over the bandwidth of the amplitude-modulated signal), therefore

$$\left|H(\omega_0 + \omega_m)\right| = \left|H(\omega_0 - \omega_m)\right| = \left|H(\omega_0)\right|, \tag{2.18}$$

then the component of the photocurrent that is retained after electrical bandpass filtering around ω_m can be written

$$i_{\omega_m}(t) = i_0 m\left|H(\omega_0)\right|^2 \cos\left(\phi(\omega_0) - \frac{\phi_+ + \phi_-}{2}\right)\cos\left(\omega_m t + \frac{\phi_- - \phi_+}{2} - \varphi\right) \tag{2.19}$$

where ϕ_+ and ϕ_- are shorthand notations for the phase shifts experienced by the upper and lower side-bands, respectively. Hence the phase difference between the detected signal and the reference signal used to drive the modulator is

$$\Delta\varphi = \frac{\phi_+ - \phi_-}{2}. \tag{2.20}$$

Equation (2.20) shows that the amplitude-modulated (AM) signal effectively probes the DUT at two frequencies corresponding to its two side-bands, and that the method effectively returns an average of the phase of the DUT at the side-bands' frequencies. If, furthermore, the phase can be assumed to vary linearly around the laser carrier frequency,

$$\phi(\omega) = \phi(\omega_0) + \frac{\partial\phi}{\partial\omega}(\omega_0)(\omega - \omega_0), \tag{2.21}$$

then the phase difference $\Delta\varphi$ can be directly related to the group delay at ω_0 according to (2.16). This last assumption is equivalent to considering the group delay constant over the bandwidth of the amplitude-modulated signal.

Equation (2.16) shows that, for a given phase resolution of the vector voltmeter or network analyser, typically of the order of 0.1°, the group delay resolution of the method can be improved by increasing the modulation frequency. However, this will result in a larger frequency separation between the side-bands of the AM signal. Consequently, the assumption that the phase of the DUT can be considered linear over the bandwidth of the amplitude modulated signal might no longer be satisfied.

The modulation phase-shift technique is widely used for the characterisation of the dispersion of optical fibres [47] where both, dispersion and attenuation, are expected to be slowly varying functions of wavelength, meaning that the assumptions of (2.18) and (2.21) are fulfilled over a frequency range up to a few gigahertz corresponding to the separation between the AM signal side-bands. However, the situation is radically different in the case of the characterisation of WDM filters where both, the dispersion and attenuation, are expected to vary significantly with wavelength, especially at the edges of the pass-band or stop-band of the device. Furthermore, as the dispersion values associated with optical filters are expected to be relatively small, the use of relatively high modulation frequencies might be required for their characterisation, hence increasing the side-bands' separation. Consequently, a compromise has to be found between group delay resolution and distortion induced by the averaging effect.

This point is illustrated in Fig. 2.6 where results of phase-shift measurements performed on a fibre Fabry–Perot filter with a FWHM bandwidth of 40 GHz are represented together with the calculated group delay response of the filter. While reasonably good agreement is obtained for a modulation

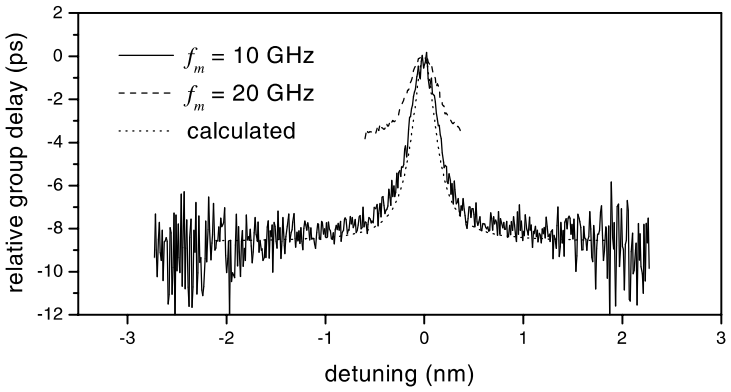

Fig. 2.6. Relative group delay of a 40 GHz fibre Fabry–Perot filter measured by the phase-shift technique using modulation frequencies of 10 and 20 GHz. The calculated group delay curve is shown for comparison. Note that raw measurement data without curve fitting nor averaging are presented

frequency of 10 GHz, this is no longer the case at 20 GHz where the measured group delay departs significantly from the theoretical value.

The relative error induced by the use of a too high modulation frequency can be assessed numerically if the theoretical group delay or dispersion responses are known. Not only the relative phase experienced by the two sidebands affects the accuracy of MPS measurements, but also their relative attenuation. Figure 2.7 shows the theoretical group delay response of a Gaussian apodised fibre Bragg grating designed for 50 GHz channel spacing (FWHM bandwidth: 44 GHz) together with simulated phase-shift measurement results that would be obtained when using modulation frequencies of 1, 5, 10, and 20 GHz. Relatively good agreement is observed between the theoretical group delay and the simulated measurement performed with a modulation frequency of 1 GHz. However, the group delay features at the edges of the passband are no longer properly characterised when the modulation frequency is increased to 5 or 10 GHz. An inversion of the variations of the measured group delay close to the passband centre frequency even appears when a modulation frequency of 20 GHz is used. In contrast to the case of a real measurement, only the choice of a too high modulation frequency affects the retrieved group delay in those simulations. In practice, the resolution of the group delay at low modulation frequencies will be limited by the phase accuracy of the vector voltmeter and the signal-to-noise ratio of the detected signal. The latter will limit the bandwidth over which accurate measurements can be performed due to the filter attenuation.

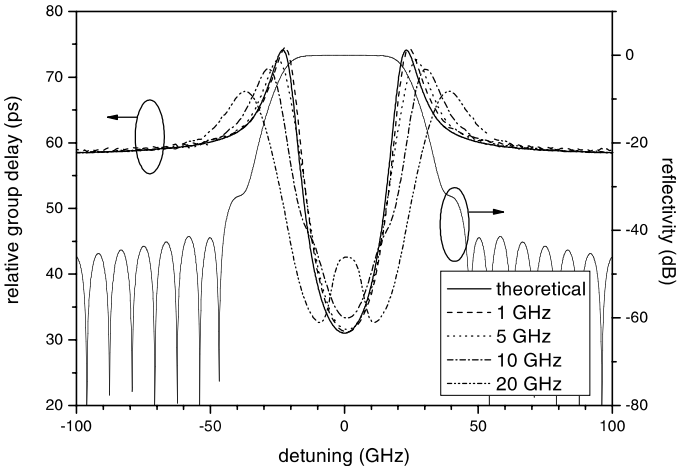

Fig. 2.7. Theoretical transfer function of a Gaussian apodised fibre Bragg grating designed for 50 GHz channel spacing and simulated group delay curves obtained with the phase-shift method using modulation frequencies of 1, 5, 10, and 20 GHz

In the case of the characterisation of the group delay ripples typically associated with fibre Bragg gratings (those will be discussed in more details in Sect. 2.4.3 as well as in Chap. 5), increasing the modulation frequency will decrease the amplitude of the measured ripples [48]. Depending on their wavelength periodicity, some modulation frequencies might even result in an inversion of the polarity of the measured group delay ripples [49].

A drawback of the modulation phase-shift method is that it enables the determination of the group delay of the device according to (2.16), and not of its dispersion. The dispersion can be obtained by numerical differentiation based on (2.16). However, the numerical differentiation of noisy measurement data turns out to be difficult unless a fitting or smoothing procedure is used [50]. Consequently, it has become customary to use a representation of the group delay as a function of wavelength to describe the measured dispersive properties of WDM filters in scientific publications or product data sheets. An adaptation of the MPS method, known as the "differential phase-shift technique" [51], uses low speed modulation of the frequency of the laser source operated in an otherwise conventional phase-shift set-up to directly detect the change in group delay occurring over the wavelength excursion of the laser $\delta\lambda$, hence enabling a direct determination of the dispersion according to

$$D(\lambda) = \frac{\Delta\varphi(\lambda + \delta\lambda/2) - \Delta\varphi(\lambda - \delta\lambda/2)}{2\pi f_m \delta\lambda}. \tag{2.22}$$

The method suffers from the same limitations as the conventional phase-shift technique regarding accuracy of the measurement of devices having strong wavelength-dependent features such as WDM filters, but it removes the need for curve fitting in order to obtain the dispersion from the measured group delay. A detailed comparison of the MPS and differential phase-shift techniques in a metrology environment can be found in [52, 53].

Enhancement of the Accuracy of the Phase-shift Technique

Since the shortcomings of the modulation phase-shift method for the characterisation of WDM filters have been realised, a number of approaches have been suggested in order to improve its accuracy.

If a single side-band (SSB) signal is substituted to the double side-band amplitude-modulated signal in a conventional phase-shift set-up, the difference between the phase of the detected signal at ω_m and the phase of the sinusoidal signal driving the modulator becomes

$$\Delta\varphi = \pm(\phi_{\pm} - \phi_0), \tag{2.23}$$

where the sign depends on the selected side-band, and ϕ_0 is the phase shift induced by the filter at the carrier frequency ω_0. Such a single side-band signal can easily be generated by creating a 90 degree phase-shift between the sinusoidal signals applied to the two arms of a dual-drive Mach–Zehnder modulator [54]. By keeping the CW laser frequency ω_0 constant and sweeping the modulating frequency, it becomes possible to directly map the phase transfer function of the device under test with high accuracy [55], including group delay ripples that would not be resolved using the conventional MPS method.

Another approach consists in locking one of the side-bands of the AM signal to a precise absolute frequency and increasing the modulation frequency simultaneously with the CW laser carrier frequency, so that the second side-band scans over the wavelength range of interest [56]. As for the SSB method, the wavelength range over which the measurement is performed is then limited by the maximum frequency at which amplitude modulation and detection are possible, typically up to a few tens of gigahertz. The characterisation of typical WDM filters will require the measurement to be repeated at different carrier frequencies or locked side-band absolute frequencies in order to scan over the full bandwidth of the device.

Post-processing of measurement data obtained using the conventional phase-shift technique has also been proposed as a way to circumvent the averaging effect of the method at high modulation frequencies. In [57] the measured group delay spectrum $\tau_{meas}(\omega)$ has been shown to be equal to the convolution of the real group delay with a rectangular function Π equal to $1/2\omega_m$ over the interval $[-\omega_m, \omega_m]$,

$$\tau_{meas}(\omega) = \tau(\omega) * \Pi(\omega/2\omega_m). \tag{2.24}$$

Fourier transforming (2.24) leads to

$$\mathrm{T}_{meas}(u) = \mathrm{T}(u)\ \mathrm{sinc}(\omega_m u), \tag{2.25}$$

where $\mathrm{T}(u)$ and $\mathrm{T}_{meas}(u)$ are the Fourier transforms of the real and measured group delay, respectively, and where the Fourier variable u is related to the inverse of the frequency period of the ripples. This approach has been successfully applied to explain the reduction of the amplitude of measured group delay ripples when the modulation frequency is increased, as well as the inversion of polarity observed for some modulation frequencies, depending on the spectral content of the ripples. However, deconvolution of measured phase-shift data is made difficult due to the zeros of the sinc function. Performing phase-shift measurements at two different modulation frequencies and using a weighted average of their Fourier transforms has been shown to overcome this difficulty [58].

Beyond the influence of the modulation frequency, other limitations of the accuracy of the MPS method such as the residual chirp of the Mach–Zehnder modulator, the phase linearity of the electrical devices when the power of the detected optical signal is varying, for instance due to the edge of the transfer function of a filter [59], or the influence of the amplified spontaneous emission noise of the laser source [60] have been pointed out. Phase drifts of the measurement system might also constitute a limiting factor, especially when either high spectral resolution characterisation is performed by using small tuning steps for the CW laser, or when high accuracy is sought at lower modulation frequencies by averaging over a large number of measurements of the electrical phase difference $\Delta\varphi$. Fast wavelength scanning has been demonstrated using continuously swept lasers [61], however, at the price of reduced wavelength accuracy due to the impossibility to use conventional wavelength meters.

In spite of its known limitations, the modulation phase-shift method has established itself as the standard for group delay measurements of WDM filters due to is relative simplicity. Careful optimisation of the measurement set-up and procedure has been shown to enable high accuracy characterisation [53, 59, 62]. It is nevertheless essential to be aware of its limitations in order to allow for a correct interpretation of MPS measurement results, as provided for instance in WDM filter manufacturers' data sheets.

The Dispersion Offset Method

The analysis of the modulation phase-shift method shows that the amplitude of the photocurrent at the modulation frequency also depends on the phase properties of the device under test through the even orders of its Taylor expansion, as can be seen in (2.19). If a second order Taylor expansion is sufficient to describe the phase around the carrier wavelength λ_0, the cosine term describing the amplitude of the photocurrent in (2.19) cancels for modulation frequencies satisfying

$$f_k^2 = \frac{(k-1/2)\,c}{D\lambda_0^2}, \tag{2.26}$$

where k is a strictly positive integer. It is therefore possible to relate the frequencies at which the magnitude of the photocurrent cancels to the value of the dispersion at the carrier frequency. Such an RF modulation method, also known as "fibre transfer function" method, has been proposed for the measurement of dispersion in optical fibres [63, 64] and can be extended to the direct characterisation of the dispersion of filters [65]. The method relies on the fact that, due to the dispersive nature of optical components, the propagation constants of the two side-bands of the amplitude-modulated

signal are different. For a given dispersion value, modulation frequencies can be found where the components of the beat signal between the carrier and the side-bands are in counterphase, resulting in cancellation of the photocurrent seen as dips in the small-signal frequency response. The experimental approach consists of sweeping the frequency of the modulating signal and detecting the cancellations of the photocurrent on a network analyser in order to measure the frequencies f_k from which the dispersion at the CW laser frequency can be calculated according to (2.26). Such a measurement can be performed by using a set-up similar to the one represented in Fig. 2.8.

From (2.26) it can be seen that the minimum dispersion that can be measured by this method depends on the maximum frequency at which the amplitude modulated signal can be generated and detected. This limitation arises from the fact that, for a given amount of dispersion, the phase mismatch between the side-bands required for cancellation of the photocurrent is only achieved when the side-band separation is large enough. For instance, a minimum dispersion of 156 ps/nm can be measured at 1550 nm if the maximum modulation frequency is 20 GHz. By inserting a constant dispersion offset, such as a length of standard single mode fibre, small values of both positive and negative dispersions can be measured, making the method suitable for the characterisation of optical filters. Such an offset will increase the total amount of dispersion to a value large enough to be measured by the set-up. The dispersion of the device under test is then equal to the change in total dispersion after it has been inserted. Stability of the dispersion offset over time should therefore be ensured, for instance by keeping it at a constant temperature.

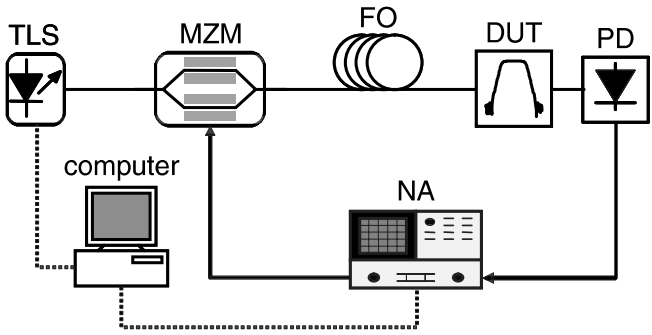

Fig. 2.8. Dispersion offset measurement set-up. TLS: tuneable laser source; MZM: Mach–Zehnder modulator; FO: fibre offset; DUT: device under test; PD: photodiode; NA: network analyser

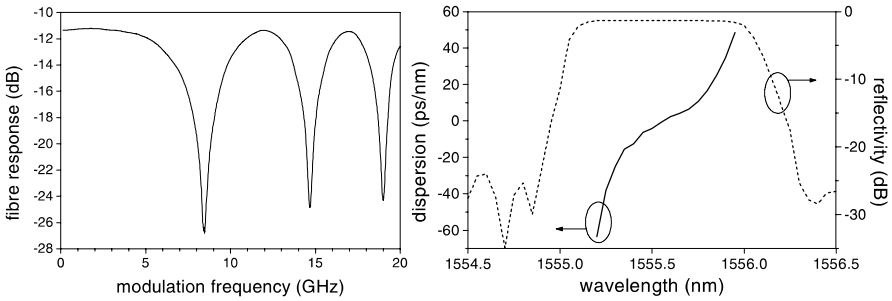

Fig. 2.9. (*Left*) measured frequency response of 50 km of standard single mode fibre. The shift of the frequency dips enables to determine small dispersion values introduced by optical components such as WDM filters. (*Right*) dispersion of a fibre grating Mach–Zehnder optical add-drop multiplexer measured with the dispersion offset technique

When characterising optical filters, the two side-bands of the AM signal might experience different attenuation. In this case, it can easily be shown [65] that imperfect cancellation of the detected signal occurs, resulting in shallower dips in the modulation transfer function, but that the frequencies of the dips are not affected by the relative amplitude of the side-bands. However, this effect limits the accuracy of the determination of the dips' frequencies. Consequently, the applicability of the method depends on the steepness of the slope of the amplitude transfer function of the filter under test.

As an example, the dispersion offset method has been applied to the characterisation of a commercial fibre grating Mach–Zehnder optical add-drop multiplexer (OADM) based on the design initially proposed in [66], showing values in excess of ±40 ps/nm in the considered wavelength range, as illustrated in Fig. 2.9.

In the remaining part of this chapter, it will be examined how the knowledge of the dispersion of optical filters can be related to their impact on transmission systems and networks, thus allowing proper selection of a filter type for a given application.

2.4 Dispersion of WDM Filters and System Implications

The dispersive properties of WDM filters have been the object of increased attention over the past few years. Consequently, those are now systematically studied, either based on measurements performed on real devices using one of the methods described in Sect. 2.3, or based on filter modelling. The phase behaviour of various WDM filter technologies has been discussed in depth in previous work [4, 5, 67], and the phase characteristics

of some of the filter types covered in the present book are presented individually in the relevant chapters. In this section, some general issues about the dispersion of optical filters and its system implications are discussed. First, the group delay behaviour of three of the most widely used WDM filter technologies (fibre Bragg gratings, multilayer interference filters, and arrayed waveguide gratings) is compared based on measurements performed on commercially available components. The system impact of filter dispersion and methods for its numerical and experimental evaluation are then reviewed. The special case of group delay ripples presented by some types of filters such as chirped Bragg gratings is treated separately. Finally, novel filter designs where additional degrees of freedom are introduced in order to simultaneously tailor their amplitude and phase responses are briefly presented.

2.4.1 Dispersive versus Linear–phase Filters

Filter technologies such as fibre Bragg gratings (Chap. 5), thin-film interference filters (Chap. 7) and arrayed waveguide gratings (Chap. 4) have a strong potential for WDM systems applications due to their versatility and design degrees of freedom. They are typically used in subsystems such as optical add-drop multiplexers and optical cross-connects (OXCs), as well as in terminal multiplexers and demultiplexers. In what follows, typical group delay curves measured on commercial devices are compared in order to highlight the characteristic features of each type of filter. All group delay curves presented here have been measured using the standard modulation phase-shift method.

One of the main advantages of the fibre Bragg grating technology is that the transfer function of the filter can be tailored by the proper choice of the distribution of the coupling coefficient along the fibre length, which is itself determined by the longitudinal effective refractive index profile. In this way it becomes possible to “square” the passband and to reduce the crosstalk level of fibre grating filters used in reflection, a process known as apodisation. Whether this process necessarily results in increased group delay at the edges of the transfer function depends on whether the filter is minimum-phase, which is not systematically the case when a fibre grating is used in reflection, as will be described in Sect. 2.4.4. For instance, a Gaussian apodisation profile can be used to simultaneously square the pass-band while maintaining an acceptable crosstalk level [26]. As an illustration, two commercial-grade devices designed for dense wavelength division multiplexing (DWDM) systems with 100 and 50 GHz channel spacing have been characterised by the phase-shift technique. The results

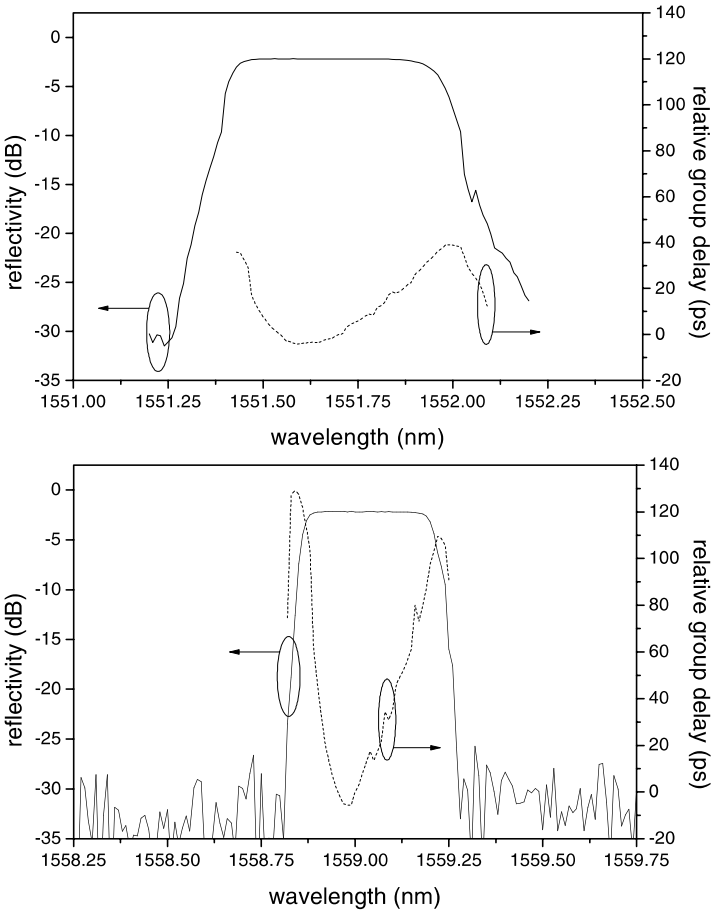

Fig. 2.10. Measured reflectivity and group delay of Gaussian apodised fibre Bragg gratings designed for 100 GHz (*top*) and 50 GHz channel spacing (*bottom*). The modulation phase-shift frequency used for the group delay measurements is $f_m = 2$ GHz

obtained with a modulation frequency equal to 2 GHz are shown in Fig. 2.10. It can be seen that the shape of the group delay curve is similar for both bandwidths. However, the extent of the variations of the group delay with wavelength is much higher in the 50 GHz grating case, indicating that this device exhibits higher values of dispersion in the passband than its 100 GHz counterpart.

Dielectric multilayer interference filters, also known as thin-film filters, consist of several Fabry–Perot like cavities separated by reflectors made of stacks of alternating low and high refractive index quarter-wave layers. The possibility to tailor their bandwidth and the steepness of the slope of

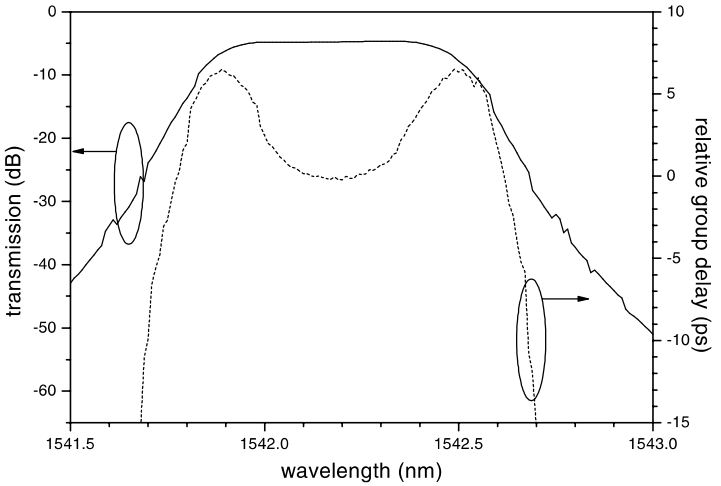

Fig. 2.11. Measured transmittivity and group delay (modulation frequency $f_m = 2.5$ GHz) of a thin-film filter-based demultiplexer

their transfer function by engineering the number of cavities and λ/4 dielectric layers makes them particularly attractive for DWDM applications [68, 69]. A typical transfer function of a thin-film (de)multiplexer is represented in Fig. 2.11, showing a characteristic flat-top and relatively steep-slope response. The 3 dB and 20 dB bandwidths of the transfer function are 80 and 120 GHz, respectively. The dispersion is equal to 0 ps/nm at the centre wavelength and is found to vary between −60 and +20 ps/nm within the 3 dB bandwidth. The dispersion behaviour of thin-film filters depends on the device structure and can also be influenced by imperfections in layer deposition resulting in non-uniformities and surface roughness [70]. As such devices can be shown to be minimum-phase in transmission [5], any attempt to square their transfer function, for instance in order to accommodate smaller channel spacing in DWDM systems, will result in increased dispersion at the edges of the passband. However, exploiting their design degrees of freedom can be used to mitigate dispersion effects while preserving an acceptable amplitude response [71, 72]. Additionally, a second stage consisting of a reflective all-pass filter can be added in order to partially compensate for the dispersion of conventional transmission bandpass filters [73] (cf. Fig. 7.7).

As pointed out in [5], the mechanism of resonant coupling in grating devices means they could be considered to the limit as being equivalent to thin-film filters with a large number of cavities. The measured group delay responses represented in Figs. 2.10 and 2.11 confirm the similar behaviour of these two types of filters, although the characterised thin-film filter

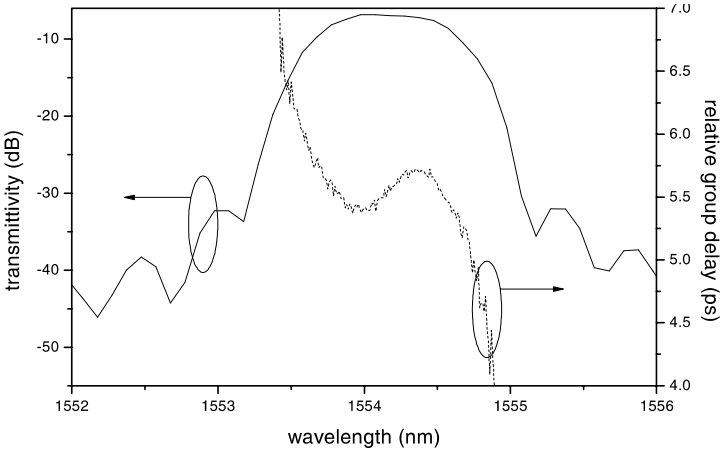

Fig. 2.12. Measured transmittivity and group delay (modulation frequency $f_m = 10$ GHz) of an arrayed waveguide grating demultiplexer designed for 200 GHz channel spacing

appears to be less dispersive than a Gaussian apodised grating of equivalent bandwidth.

Arrayed waveguide gratings consist of two free-propagation regions to which the input and output fibres are connected, linked by an array of waveguides designed in such a way that the optical length difference between two consecutive waveguides is constant [74, 75, see also Chap. 4]. Those devices can be used as (de)multiplexers as well as wavelength routers. It can easily be shown that, if the distribution of the excitation of the arrayed waveguides is symmetric, then an AWG is a linear-phase device, consequently dispersion-free [5, 67].

Figure 2.12 shows the measured power transfer function and group delay of a conventional (i. e. whose passband has not been flattened by some of the techniques discussed briefly in Sect. 2.4.4 as well as in Chap. 4) AWG designed for 200 GHz channel spacing and having a 3 dB bandwidth of 125 GHz. A modulation frequency as high as 10 GHz was necessary in order to be able to measure the group delay in the passband, indicating that the device exhibits low dispersion values. At such a high modulation frequency, the limitations of the measurement method described in Sect. 2.3.2 should be kept in mind. The maximum dispersion value in the passband is estimated to be ±2 ps/nm, confirming the nearly linear-phase nature of conventional non passband flattened AWGs.

The origin of residual dispersion has been investigated in AWG multiplexers with a Gaussian spectral response, as well as for passband flattened devices [42]. Phase and amplitude errors in the transmission of the arrayed waveguides have been identified as the main source of the dispersion. Fourier

transform spectroscopy measurements performed on InP and silica-on-silicon devices showed that slowly-varying phase errors (i. e. non-random contributions to the phase distribution of each path in the arrayed waveguides) were responsible for dispersion imperfections [43, 76], as confirmed by device modelling [77].

The three examples shown above highlight the importance of the choice of a proper technology if the dispersive properties of DWDM filters are relevant. The degrees of freedom offered by apodisation of fibre Bragg gratings enable to realise nearly ideal flat-top transfer functions offering low adjacent channel crosstalk and reduced passband narrowing when cascaded, however, at the expense of dispersion at the edges of the passband. This has been shown to be even more critical for narrow bandwidth devices necessary to accommodate reduced channel spacing. On the other hand, concepts such as AWGs do theoretically offer dispersion-free devices (in practice limited by manufacturing imperfections resulting in amplitude and phase errors between the arrayed waveguides) at the expense of a less ideal amplitude transfer function. It will be shown in Sect. 2.4.4 how extra degrees of freedom can be introduced for advanced components design in order to mitigate those usual trade-offs. Even though their properties have not been detailed in this section, it is essential to keep dispersion in mind for the other filter technologies presented elsewhere in this book, including bulk grating based devices [78, 79], ring resonators [80], and wavelength interleavers [81].

2.4.2 System Impact of WDM Filter Dispersion

Since it has been realised that the dispersion of optical filters might affect the performance of WDM systems [2, 3], a number of theoretical, numerical, and experimental studies attempting to assess the impact of filter dispersion have been reported. Such investigations aim at either getting a better understanding of the impact of a given complex transfer function on the quality of the filtered signal, hence potentially enabling to optimise the design trade-offs for the amplitude and phase responses, or at assessing the tolerances or scalability limitations of optical links or networks making use of such filters.

From a component design point of view, the focus is on evaluating signal distortion induced by the combined effects of the amplitude and phase responses, in order to assess whether it is possible to reach a desired amplitude response target while keeping the phase induced distortion under control. In the case of wavelength (de)multiplexers, a so-called flat-top transfer function, presenting low adjacent channel crosstalk level, reduced bandwidth

narrowing when cascaded, as well as small dispersion values at the passband edges will be sought. In other types of filtering elements such as dispersion compensating devices, the target will be to achieve a desired dispersion profile over a given bandwidth while minimising the effects of undesired group delay variations known as group delay ripples (cf. Sect. 2.4.3).

Optical network designers will have interest in determining the maximum number of devices that can be cascaded over a link, hence the number of nodes over which a signal can be routed transparently without resorting to optical or electro-optic regeneration [82]. Clearly, this number will depend on the rate at which the effective bandwidth of a cascade of filters decreases, justifying the need for flat-top transfer functions that are more resilient to bandwidth narrowing, but also on the dispersion accumulated over the path, including filter-induced dispersion. Additionally, the knowledge of system margins is of paramount importance for the design of all-optical WDM networks. These margins include the tolerance to misalignment between the signal centre frequency and the centre frequencies of the filters present along the link, which may be limited by the dispersion at the edges of the filters' passbands.

It is therefore essential to be able to evaluate dispersion-induced limitations arising because of WDM filters. Together with other key filter parameters such as:

- insertion loss,
- passband shape,
- adjacent channel crosstalk,
- in-band crosstalk for devices such as wavelength routers,
- polarisation-dependent loss and polarisation mode dispersion,
- thermal and mechanical stability,

the knowledge of the dispersive properties of a given filter and its system implications will help assessing the suitability of this particular filter technology to the system under design.

It is beyond the scope of this chapter to present results on dispersion-induced signal degradation for all the filter technologies presented elsewhere in this book. Those will depend not only on the filter type, but also on its practical realisation, as well as on numerous system parameters, including bit-rate, modulation format, signal extinction ratio, and chirp. Consequently, such results will not be general enough to be of significant value, and general trends of the dispersive behaviour of the most widely used filter technologies have already been presented in Sect. 2.4.1. Instead, general techniques used to evaluate the influence of WDM filter dispersion on signal degradation are introduced and illustrated by specific examples.

Many of the early demonstrations of the impact of filter dispersion refer to fibre gratings. Some of the first evaluations of the dispersion-induced limitation of the usable bandwidth of grating filters have been performed by assuming a maximum tolerable value of dispersion, for instance 1000 ps/nm corresponding to about 1 dB power penalty for a 10 Gbit/s non-return-to-zero (NRZ) system [83]. By calculating the grating complex transfer function, typically by using a transfer matrix approach based on coupled-modes equations [84], it becomes possible to evaluate the frequency range over which the filter dispersion remains within this limit [85]. While such an approach enables to easily link grating design parameters (such as the apodisation function, grating length, and refractive index modulation value) to a system related quantity (the grating usable bandwidth), it ignores the interaction between amplitude and phase filtering as well as the fact that the dispersion may vary significantly over the modulated spectrum width, especially at the edges of the filter passband. Consequently, more accurate system modelling is required in practice. Calculating the amount of broadening experienced by a single Gaussian pulse has been used to evaluate the dispersive behaviour of a chirped moiré grating exhibiting almost constant in-band group delay [86]. However, in digital optical communication systems, a linear device such as an optical filter may introduce intersymbol interference, and it is therefore desirable to evaluate its effect on a whole data pattern, usually modelled as a pseudo-random bit sequence (PRBS). It is customary to resort to numerical simulation in order to calculate the complex envelope of a modulated signal after it has been filtered by one or a cascade or WDM filters. In the absence of suitable receiver models able to properly evaluate the bit-error-rate (BER) of signals strongly deteriorated by intersymbol interference, qualitative comparisons based on calculations of the eye-opening penalty (EOP) are often used. However, such a figure of merit is difficult to relate to the BER-based quantities, such as power penalty, that are used in practice to define the system margins.

It is therefore preferable, whenever possible, to perform an experimental evaluation of the filtering-induced signal degradation. Such early investigations have been reported for instance in [87, 88] for a single apodised fibre Bragg grating used in reflection or in transmission. The influence of the chirp of a 10 Gbit/s NRZ modulated signal was further investigated. Asymmetries in the penalty against wavelength detuning curves for chirped signals enabled to conclude on the influence of the grating dispersion that exhibits opposite signs on the short and long wavelength sides of the passband. A first experimental comparison of the power penalty induced by a fibre Bragg grating and an arrayed waveguide grating filter was presented in [89], clearly outlining the inherent dispersive limitations of

fibre gratings as opposed to linear phase devices [90]. Other early reports on the evaluation of the system impact of filter dispersion include penalty measurements in transmission and reflection for a single tuneable grating [91]. As an illustration, Fig. 2.13 shows the measured penalty as a function of wavelength for a 10 Gbit/s NRZ signal reflected by a Gaussian apodised FBG designed for 50 GHz channel spacing. The usable bandwidth for a maximum tolerable power penalty can be determined from such a measurement. However, distinguishing the relative contribution of phase and amplitude filtering is difficult. Numerical simulations, where it is possible to independently calculate the effect of amplitude, phase, and conjugated filtering, might provide qualitative insights into the main source of signal degradation and can be used to complement such penalty measurements.

When a fibre grating is used in transmission, as is typically the case in optical add-drop multiplexer structures, either using optical circulators [92] or in a Mach–Zehnder interferometer configuration [66] (cf. Figs. 5.28 and 5.29), its out-of-band dispersion might induce degradation to the channels that are immediately adjacent to the dropped one. This might ultimately limit the channel spacing in DWDM networks making use of such devices. This potential limitation was recognised in [93] where a single Gaussian pulse analysis was performed based on an analytical expression for the out-of-band dispersion of a grating used in transmission. An evaluation of grating dispersion in transmission and its consequence on pulse degradation was also performed in [94, 95] where the use of the grating in

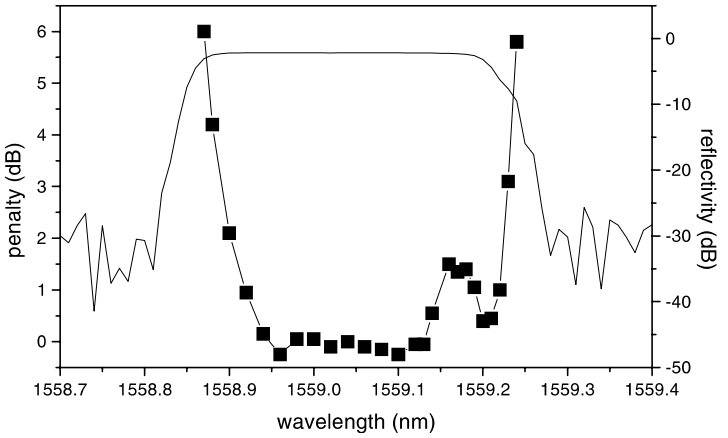

Fig. 2.13. Power penalty (at a BER of 10^{-9} – non-preamplified receiver) for a 10 Gbit/s NRZ signal reflected by the fibre grating designed for 50 GHz channel spacing whose complex transfer function is represented in Fig. 2.10. The conjugate effects of amplitude and phase filtering are accounted for in the penalty curve. Black squares: power penalty, full line: reflectivity

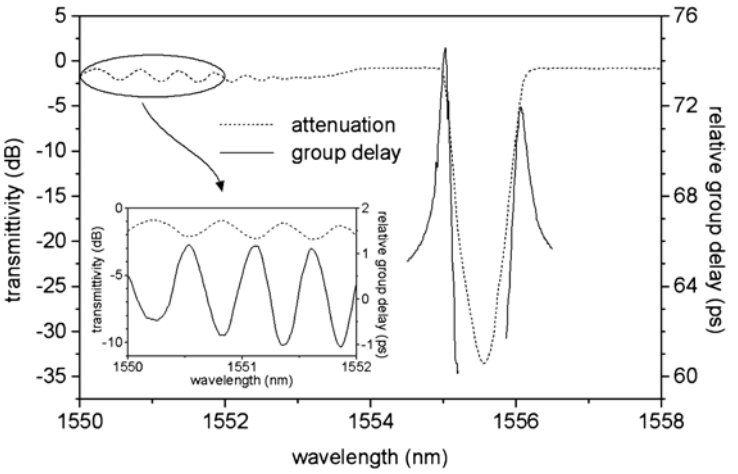

Fig. 2.14. Measured transmittivity and relative group delay in transmission of a fibre grating Mach–Zehnder OADM. The group delay around the stop-band was measured at a modulation frequency of $f_m = 5$ GHz, while $f_m = 2.5$ GHz was used to characterise the group delay associated to the amplitude ripples on the short wavelength side (inset)

an OADM was considered. The cascadability of Gaussian apodised gratings was also investigated in [96] based on an analytical expression for the out-of-band dispersion and a maximum tolerable value of dispersion. The fact that fibre gratings are minimum-phase filters in transmission has also been exploited to provide bounds on their dispersion and to examine the consequences for grating design [97]. Figure 2.14 shows the group delay of a fibre grating-based Mach–Zehnder OADM close to its stop-band. No dispersion impairments are expected if this device is used in a WDM system with 200 GHz (1.6 nm at 1550 nm) channel spacing. However, operation with 100 GHz channel spacing would result in dispersion of the order of ±5 to ±15 ps/nm for the closest channels on both sides of the stopband. The attenuation and group delay ripples observed on the short wavelength side of the stop-band will be discussed in Sect. 2.4.3.

As already mentioned, for network and system design, it is often desirable to know not only the impact of a single WDM filter on signal distortion, but also that of a full cascade of filters, as encountered by the signal propagating along a given path in the network. In this case the full range of analytical and numerical techniques described previously remains available [95]. For instance, in [6] it was found that dispersion accumulation is the main limitation to the cascadability of flat-top FBGs and thin-film filters. Approximating the dispersion at the centre of the passband with a linear function of wavelength enabled to numerically assess the detuning tolerance of a cascade of filters for a given value of power penalty.

From the experimental side, transmission over a filter cascade can be emulated by re-circulating loop experiments where the signal is propagated a number of times through a single component. One obvious limitation to the scheme is that it emulates propagation through perfectly aligned filters having strictly identical transfer functions which is certainly not the case in a real network. However, unless one is able to do experiments on a specific link or path through a network, taking into account the relative detuning of the filters as well as manufacturing-induced differences between their transfer functions would require a statistical treatment in order to obtain results of a sufficiently general value, especially when the system is made nonlinear due to propagation over optical fibre spans. Other known limitations of re-circulating loop experiments are the extra loss induced by the loop switch, as well as the fact that some length of fibre is necessary to store data into the loop. Consequently, if one is interested in evaluating the degradation induced by the filter alone, it should be ensured that this fibre span is perfectly dispersion-compensated and operated in the linear regime. In spite of these limitations, re-circulating loops are convenient tools to emulate filtering-induced degradation in large scale WDM networks when only a few filter samples are available, as would be the case for device prototyping.

Such an approach has been used in [3] to successfully demonstrate that the cascadability of WDM filters is also influenced by their dispersive characteristics. The detuning tolerance of dispersive multilayer interference filters was found to be less than half that of dispersion-free AWG designs. In Fig. 2.15 it is shown how the usable bandwidth of the fibre Bragg grating designed for 50 GHz channel spacing, whose transfer function is represented in Fig. 2.10, narrows when the device is cascaded up to 5 times in a re-circulating loop. Furthermore, its optimum operation wavelength is shifted towards the short wavelength side of its passband (1558.98 nm) corresponding to an extremum of the group delay curve, hence zero-dispersion [98].

Another reported approach has consisted in measuring the power penalty induced by a single grating, and after ensuring good agreement with simulations, numerically extrapolating the results to a cascade of filters [99]. Straight line experiments aiming at evaluating the power penalty induced by a cascade of FBGs have also been reported [100]. In [101], an experimental and numerical comparison of the power penalty induced by cascading fibre Bragg gratings and thin-film filters was further conducted. It was confirmed in this study that the dispersion of the gratings was largely responsible for the measured penalty. More recently, a detailed comparison of the cascadability behaviour of conventional Blackman apodised gratings with dispersion-optimised designs has confirmed the

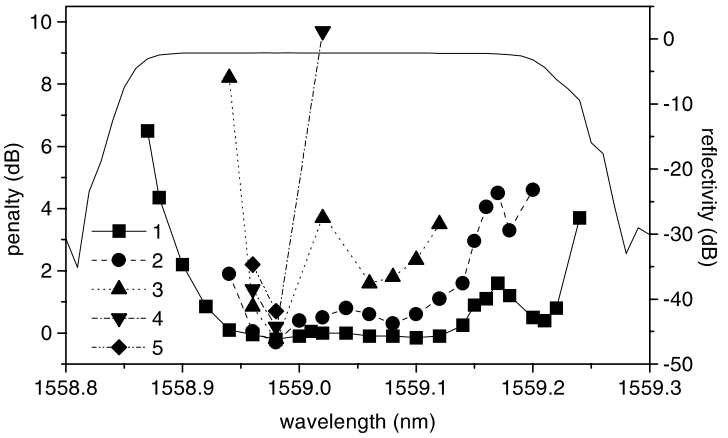

Fig. 2.15. Power penalty as a function of wavelength for 1 to 5 round trips in a recirculating loop set-up where a 10 Gbit/s NRZ signal is reflected by a Gaussian apodised FBG designed for 50 GHz channel spacing

importance of proper dispersion engineering for high bandwidth utilisation in FBG-based devices [102].

The use of vestigial side-band (VSB) filtering has enabled the demonstration of DWDM systems with high spectral efficiency and record capacity [103]. In such schemes the redundancy of the information contained in the two side-bands of e. g. an NRZ signal is exploited in order to reduce the channel spacing after partial suppression of one of the side-bands by optical filtering. In contrast to the conventional use of filtering elements as (de)multiplexers, the edge of the passband of optical filters is now used to effectively suppress the undesired side-band. Alternatively, a notch filter can be used for the same purpose [104]. In both cases, the need for a sharp filter cut-off necessary in order to obtain good side-band suppression may cause the preserved side-band to experience significant dispersion, depending on the filter technology. Consequently, a trade-off between the side-band suppression ratio and the dispersion-induced pre-chirping of the signal needs to be considered since both result from the steepness of the VSB filter transfer function [105]. The negative dispersion associated with the short wavelength edge of the passband or stopband of a fibre grating might actually contribute to the observed enhanced dispersion tolerance of VSB signals whose corresponding side-band has been suppressed, as observed in [104]. To illustrate this point, the eye-opening penalty of a filtered 10 Gbit/s NRZ signal has been calculated for various values of the detuning of its centre frequency with respect to the centre of the passband of a Gaussian apodised FBG designed for 50 GHz channel spacing. The results are shown

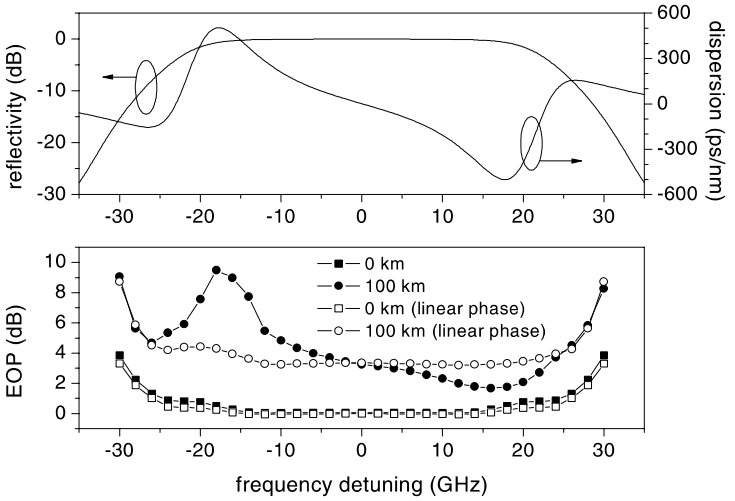

Fig. 2.16. Top: calculated transfer function (reflectivity and dispersion) of a Gaussian apodised fiber Bragg grating designed for 50 GHz channel spacing. Bottom: eye-opening penalty as a function of NRZ signal detuning with respect to the grating centre frequency. The EOP was calculated using a 2^{10}–1 pseudo-random sequence directly after the VSB filter (0 km) and after transmission over 100 km SMF. For comparison, EOPs have also been calculated assuming the VSB filter is linear-phase

in Fig. 2.16 for transmission over 100 km standard single mode fibre, as well as directly at the output of the VSB filter. For comparison, the corresponding eye opening penalties have also been calculated with a hypothetical VSB filter whose amplitude transfer function is the same as that of the FBG, but exhibiting no dispersion (linear-phase filter). It is clearly seen that, beyond reduction of the signal spectral width potentially allowing for increased spectral efficiency, the negative filter dispersion is mostly responsible for the enhanced dispersion tolerance observed for positive frequency detunings. Consequently, the dispersion of the VSB filter needs to be taken into account for the proper design of such systems, as outlined in [104], as well as in [106] where a low dispersion bulk diffraction grating multiplexer was used for side-band suppression.

2.4.3 Group Delay Ripples

Fast oscillations of the group delay of an optical filter with respect to wavelength are usually referred to as group delay ripples (GDR). Here, fast oscillations means that their frequency period is small compared to the filter bandwidth and to the average trend of the group delay change within

the filter passband. Such ripples can be found in a number of resonant WDM filter types including chirped fibre Bragg gratings used for dispersion compensation [107] or for gain equalisation [108], long period fibre gratings [109], and various structures of all-pass filters designed for dispersion compensation [110, 111]. The amplitude and periodicity of the GDRs depend on the filter design as well as on imperfections in the fabrication process. In the following, GDRs are illustrated in more detail in the context of chirped fibre Bragg gratings. However, the subsequent discussion on their impact on optical fibre communication systems holds independently of the filter technology.

In the case of FBGs, group delay ripples occur due to interference induced by reflections at the grating ends [112]. Those ripples can therefore be reduced by a proper apodisation of the grating [107, 113], cf. also Chap. 5. Furthermore, imperfections in the fabrication process are responsible for random variations of the period and amplitude of the grating refractive index modulation that also induce GDRs through residual multiple reflections [114, 115]. Consequently, beyond the optimisation of the apodisation profile, improvements in the fabrication process are also necessary in order to allow better control of GDRs in chirped fibre gratings [116].

Figure 2.17 shows the attenuation and group delay (measured using the phase shift technique with a modulation frequency of 130 MHz) of an early chirped FBG. The average dispersion of the device (obtained from the slope of a linear fit to the measured group delay as a function of wavelength over the 1555.0 to 1555.4 nm range) is of the order of −800 ps/nm,

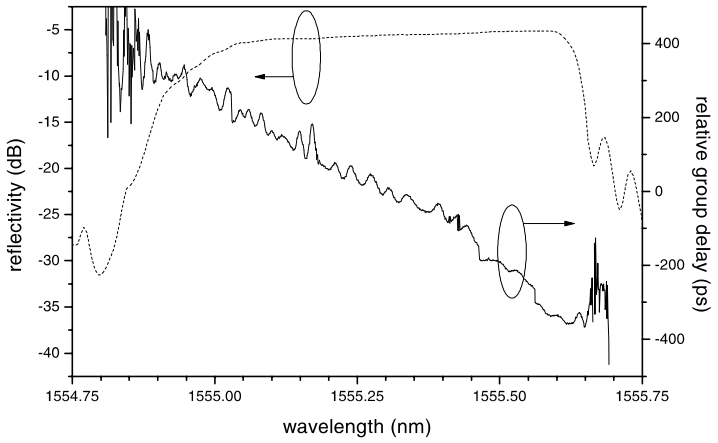

Fig. 2.17. Measured reflectivity and relative group delay of an early chirped fibre Bragg grating for dispersion compensation, showing typical group delay ripples associated with this type of component

enabling compensation of the dispersion accumulated over about 50 km of standard single mode fibre. GDRs with a period of about 4 GHz and peak-to-peak amplitude of up to several tens of picoseconds are clearly visible, resulting in large variations of the local dispersion. This example is provided for illustrative purpose only as contemporary chirped FBGs exhibit much lower GDRs thanks to optimised apodisation and improved fabrication techniques.

In order to specify the amount of GDR that can be tolerated for a given system, it is essential to be able to assess its influence on the filtered signals. The impact of GDRs on system performance is difficult to predict since it depends on their amplitude, period (relative to the signal spectral width), and phase (with respect to the channel centre frequency). The purpose of a typical chirped FBG is to compensate for the dispersion accumulated by the signal over propagation in optical fibre. Consequently, provided higher order dispersion effects can be ignored in the fibre, a linear dependence of the group delay of the FBG with respect to wavelength is expected. Any departure from this situation is likely to result in unwanted signal distortion. For instance, a signal tuned close to the quadrature point of a sinusoidal group delay ripple having a frequency period sufficiently large compared to the bit rate will experience nearly constant dispersion, while the effect will be equivalent to that of higher order dispersion in case the signal is tuned close to an extremum of the ripple [117, 118]. Consequently, the ripple will be responsible for the creation of echo pulses that may interact with neighbouring information bits, hence leading to intersymbol interference. This point is illustrated in Fig. 2.18, where the effect of a sinusoidal GDR on an isolated raised cosine pulse has been calculated for three different relative detunings between the ripple and the centre frequency of the pulse spectrum. In the case of a sinusoidal GDR, the delay of the echo pulses can be shown to be equal to the inverse of the frequency period of the ripple. The worst case signal degradation is then induced by GDRs whose period is close to the bit rate [118–120]. Beyond this qualitative understanding some figure of merit needs to be found in order to be able to quantify the effects of GDRs [121]. The problem is complicated by the fact that the ripples of real fabricated components are not sinusoidal and that, as pointed out earlier, the induced system penalty depends also on the phase and amplitude of the ripple.

Numerous theoretical and numerical studies have contributed to a better understanding of the effects of the different relevant GDR parameters such as peak-to-peak amplitude, frequency, and phase (on top of some of the previous references, some relevant discussions can be found in e. g. [122–124]). It was shown in [125] that the peak-to-peak value of the phase ripple over the signal bandwidth (as opposed to that of the group delay

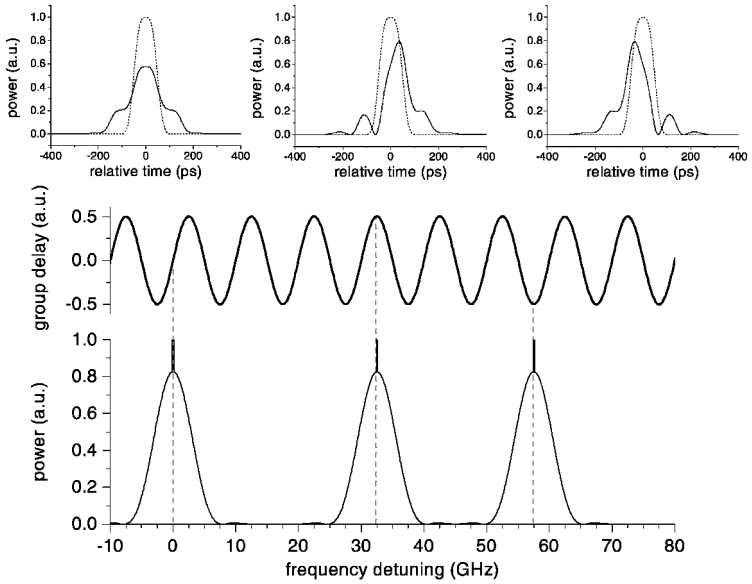

Fig. 2.18. Calculated illustration of the effect of a sinusoidal group delay ripple on an isolated pulse depending on the phase of the ripple with respect to the modulated spectrum centre frequency. The dotted line represents the pulse shape at the filter input. Here, the pulse spectral width compared to the GDR period means that the pulse will experience higher order dispersion even when the signal is tuned to the quadrature point of the ripple. In this example, an arbitrarily high value of the peak-to-peak GDR (100 ps) has been used in order to enhance its effect

ripple) could be used to accurately predict the worst case penalty experienced by the filtered signal, even in the presence of realistic GDR profiles. A method enabling the direct determination of the phase ripple with high resolution was subsequently proposed [126]. Good correlation between system performance and two figures of merit that can be extracted from GDR measurements (the residual dispersion and the variance of the residual phase ripple in the signal bandwidth) has also been reported in [127]. Ultimately, as in the general case for dispersive devices discussed in Sect. 2.4.2, experimental investigations can be performed to assess the real impact of GDRs on the performance of a fabricated filter [128, 129]. Furthermore, as the GDRs induced by imperfections in the fabrication process are not reproducible from one device to another, investigations of cascaded filtering, e. g. when chirped FBGs for dispersion compensation are used in multi-span systems, require some form of statistical analysis [130].

Coupling to cladding modes is responsible for amplitude ripples on the short wavelength side of the transfer function of fibre gratings used in transmission [26, 131], as can be observed on the measured transfer function

of an early FBG Mach–Zehnder OADM depicted in Fig. 2.14. Such amplitude ripples are associated with group delay ripples having the same periodicity, as shown in the inset of Fig. 2.14. In this particular case, the period of the ripples is estimated to be about 0.5 nm around 1551 nm, and the maximum dispersion values are ±15 ps/nm. The evaluation of system impairments related to those dispersion and amplitude ripples would require statistical considerations on their amplitude, periodicity, and phase, as well as on the topology and wavelength assignment of the WDM network where such OADMs would be used. Fortunately, techniques exist that can successfully suppress these short-wavelength ripples [132, 133].

2.4.4 Advanced Filter Design

Optical filters for WDM systems have to satisfy a number of system requirements. As discussed previously, those include low out-of-band crosstalk, large detuning tolerance in order to allow for possible system drifts, as well as low dispersion, especially when multiple filtering elements are encountered by a signal over its path in a transparent network domain. Depending on the filter technology, it might be contradictory to attempt to achieve several of those goals simultaneously. For instance, approaching a flat-top power transfer function is a desirable feature for a wavelength (de)multiplexer as it results in low adjacent channel crosstalk as well as reduced passband narrowing due to cascading. However, if the filter is minimum-phase, increased dispersion at the edges of its passband will result from the action of squaring its amplitude response. Inversely, conventional arrayed waveguide grating (de)multiplexers have been shown to exhibit very low dispersion in their passband. Unfortunately, their amplitude response can be well approximated by a Gaussian transfer function [75], and consequently exhibits smooth roll-off, making them prone to severe passband narrowing when concatenated over a given path in a network.

In this section, the implications of those design trade-offs on filter dispersion are illustrated based on two examples. First, the effect of passband flattening of AWGs on their dispersive properties is examined. Second, it is shown how advanced apodisation profiles can be used in order to reduce the dispersion of fibre Bragg gratings while maintaining their ideal square amplitude response.

Passband-flattened AWGs

Several methods have been proposed in order to approximate the desired flat-top transfer function for AWGs [134–138]. One promising approach

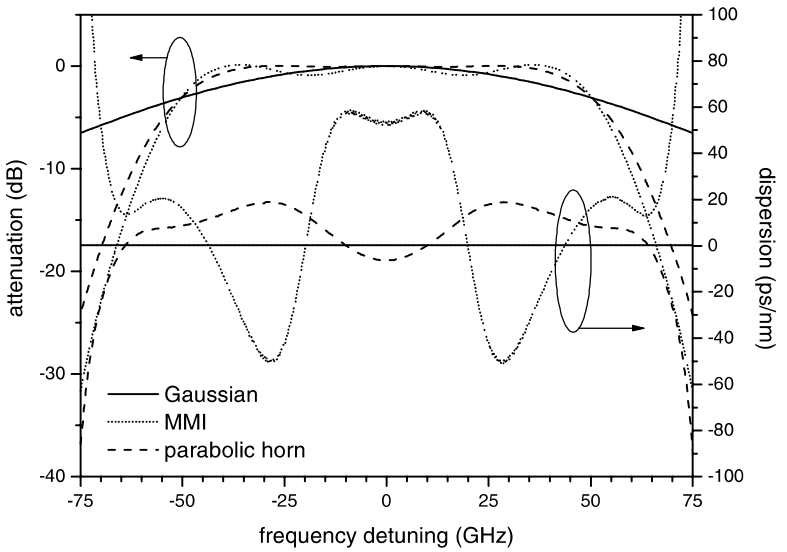

Fig. 2.19. Calculated power transfer function and group delay of a conventional Gaussian and of passband-flattened AWGs using an MMI coupler or a parabolic horn. The three devices are designed for the same 3 dB bandwidth of 100 GHz (device modelling by Chrétien Herben, METEOR project)

consists in approximating a flat-top response by the summation of two Gaussian distributions. This principle can be realised in practice by using a multi-mode interference (MMI) coupler [139] before the input slab, as proposed in [140, 141]. Alternatively, using a parabolic horn before the input slab has also been shown to result in passband flattening, as proposed in [142]. These last two approaches are the ones considered here. Issues to take into account when introducing a passband flattening process in the design of an AWG (de)multiplexer are the possible presence of ripples in the amplitude response, the introduction of excess loss, as well as the introduction of dispersion [143].

Numerical simulations have been performed to compare the dispersion properties of devices having the same 3 dB bandwidth. The results of accurate device modelling are shown in Fig. 2.19 for a conventional Gaussian, as well as for AWGs whose passbands have been flattened by using either an MMI coupler or a parabolic horn at the input of the free propagation region.

As expected, the standard Gaussian design is dispersion-free, whereas relatively large dispersion values are observed in conjunction with ~1 dB amplitude ripples when an MMI coupler is employed to square the field distribution before the input slab. Clearly, such high dispersion values

would be unacceptable for high bit rate applications and the large amplitude ripple would also prevent cascading the device. Using a parabolic horn, both amplitude ripple and dispersion are reduced. Further, a proper design of the parabolic horn has been shown to result in flat-top transmission with reduced chromatic dispersion [144]. Low dispersion passband flattened designs based on engineering the relative attenuation and phase shifts of the arrayed waveguides have also been demonstrated [145].

Low Dispersion Fibre Bragg Gratings

Since fibre Bragg gratings are compact, low-loss devices that are inherently compatible with optical fibres, considerable interest exists for realising advanced transfer functions that would present a rectangular passband in conjunction with linear phase.

It can be shown that, in the weak coupling regime, the coupling potential due to the refractive index corrugation $\kappa(z)$, where z is the longitudinal coordinate of the grating, and the reflectivity are related by a Fourier transform-like expression [146]. Although this relation no longer holds for strong gratings, it can nevertheless provide some rough design guidelines for the optimisation of the shape of the reflectivity of grating filters. The coupling potential $\kappa(z)$ depends directly on the amplitude and phase of the refractive index perturbation [147]. Therefore, in order to achieve a flat-top transfer function, the refractive index profile should follow a $\sin z/z$ dependence. However, this requires the ability to synthesise π phase-shifts in the refractive index profile. Gratings realised following this approach have been shown in [148] to exhibit far less dispersion than gratings with conventional Gaussian apodisation profiles. The use of other symmetric refractive index profiles with phase-shifts has enabled the demonstration of filters with square amplitude response and reduced dispersion [149, 150].

It has been mentioned in Sect. 2.2.2 that grating filters are generally not of the minimum-phase type when used in reflection. This opens the possibility to achieve the double goal of synthesising devices with an ideal rectangular transfer function and low dispersion at the edges of the passband. However, it has also been demonstrated in [20] that, if the grating is symmetric, its group delay is identical in transmission and in reflection. A grating being minimum-phase in transmission [20], the group delay in reflection of a symmetric device is then uniquely determined by its reflectivity. Therefore, using an asymmetric refractive index profile offers additional degrees of freedom for the design of low dispersion filters with nearly square amplitude responses. In [151–154] asymmetric refractive index profiles with multiple phase-shifts have been demonstrated, allowing

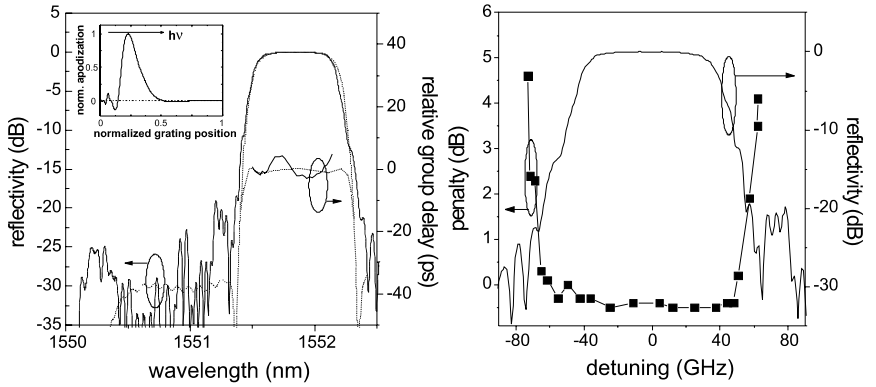

Fig. 2.20. (*Left*) measured (*solid line*) and calculated (*dotted line*) reflectivity and group delay of a low dispersion fibre Bragg grating whose normalized apodisation profile is shown as inset. (*Right*) measured penalty as a function of detuning for 10 Gbit/s return-to-zero (RZ) modulation [157]. Device modelling and characterisation by Hans-Jürgen Deyerl

the fabrication of nearly dispersion-free, high reflectivity, rectangular gratings. However, unlike the symmetric designs presented above, the dispersion-free operation of those filters is dependent on the direction of light propagation. Consequently, they may not be used in conventional OADM structures. The development of advanced grating writing techniques, together with efficient algorithms enabling to calculate the required refractive index profile to achieve a given target filter response [155], have allowed the fabrication of grating structures where both amplitude and phase responses can be engineered [156].

Figure 2.20 shows the asymmetric apodisation profile of a low dispersion fibre Bragg grating [157]. The grating was fabricated using the polarisation control method [158], and its measured reflectivity and group delay are represented together with simulation results. A reflectivity of 99.7% for a 20 mm long device as well as a group delay fluctuation of less than 10 ps were obtained within the 3 dB bandwidth of a device designed for 100 GHz channel spacing. The good dispersion properties of the grating were confirmed by penalty measurements at 10 Gbit/s, showing that up to 99% of the filter's 20 dB bandwidth could be used with less than 1 dB power penalty.

Consequently, recent results have demonstrated that advanced asymmetric refractive index profiles with multiple phase shifts can be used in order to simultaneously realise nearly ideal square amplitude responses with low dispersion.

2.5 Conclusion

In this chapter, the need for accurate determination of the dispersive properties of WDM filters and estimate of their impact on systems has been highlighted. Over the past few years, the awareness of both component and system designers towards this sensitive issue has grown, and it is now customary to present group delay curves and specifications together with the amplitude response of optical filters.

From the characterisation side, two key experimental methods, namely low coherence interferometry and the modulation phase-shift technique, have been presented in detail and their benefits and limitations discussed. These limitations should be kept in mind when analysing group delay curves found in the literature and product descriptions.

Beyond component characterisation, it is also essential to be able to quantify the effect of filters' complex transfer functions on the signal quality in an optical link or network. It has been reviewed how the in-band dispersion of WDM filters may limit the usable bandwidth of the devices as well as the number of devices that can be cascaded along a given path in a network. For some types of components, group delay ripples might induce some further signal degradation. The out-of-band dispersion in OADMs might also limit the channel spacing in DWDM systems.

Improved component manufacturing techniques are effective at reducing spurious dispersive effects due to e. g. group delay ripples or coupling to cladding modes which were critical in early generations of devices. However, basic physical limitations will remain which result from the fact that various filters are of minimum-phase type, and hence have dispersive properties fully determined by their amplitude response. It has also been illustrated how the introduction of extra degrees of freedom can be used to circumvent some of the limitations of conventional filter designs, allowing the realisation of advanced WDM filters whose amplitude and phase responses can be engineered to meet specific targets inferred from system requirements.

There is no reason to doubt that the increase in capacity needs observed since the dawn of optical communications will stop in the near future, meaning that the limits of high bit-rate and high spectral efficiency systems will need to be pushed further. Visions of complex transparent optical networks may also come closer to reality. These trends will make the requirements for understanding and control of dispersion in WDM filters even more important.

References

1. G. P. Agrawal: *Fiber-optic communication systems*, Chap. 2 (Wiley, New York, 1997)
2. N. N. Khrais, F. Shehadeh, J.-C. Chiao, R. S. Vodhanel, and R. E. Wagner: "Multiplexer eye-closure penalties for 10 Gb/s signals in WDM networks," *Techn. Digest Opt. Fiber Commun. Conf. (OFC'96)*, San Jose, California, USA, PD33 (1996)
3. C. Caspar, H.-M. Foisel, C. v. Helmolt, B. Strebel, and Y. Sugaya: "Comparison of cascadability performance of different types of commercially available wavelength (de)multiplexers," Electron. Lett. **33**, 1624–1626 (1997)
4. G. Lenz, B. J. Eggleton, C. K. Madsen, C. R. Giles, and G. Nykolak: "Optimal dispersion of optical filters for WDM systems," IEEE Photon. Technol. Lett. **10**, 567–569 (1998)
5. G. Lenz, B. J. Eggleton, C. R. Giles, C. K. Madsen, and R. E. Slusher: "Dispersive properties of optical filters for WDM systems," IEEE J. Quantum Electron. **34**, 1390–1402 (1998)
6. M. Kuznetsov, N. M. Froberg, S. R. Henion, and K. A. Rauschenbach: "Power penalty for optical signals due to dispersion slope in WDM filter cascades," IEEE Photon. Technol. Lett. **11**, 1411–1413 (1999)
7. L. G. Cohen: "Comparison of single-mode fiber dispersion measurement techniques," J. Lightwave Technol. **LT-3**, 958–966 (1985)
8. P. Hernday: "Dispersion measurements," in *Fiber Optic Test and Measurement* (D. Derickson, ed.), Chap. 12 (Prentice Hall, Upper Saddle River, NJ 1998)
9. W. H. Knox, N. M. Pearson, K. D. Li, and C. A. Hirlimann: "Interferometric measurements of femtosecond group delay in optical components," Opt. Lett. 13, 574–576 (1988)
10. A. Papoulis: *The Fourier integral and its applications*, Chap. 10 (McGraw-Hill, New York, 1962)
11. H. W. Bode: *Network analysis and feedback amplifier design*, (Van Nostrand, New York, 1945)
12. L. D. Landau, E. M. Lifschitz, and L. P. Pitaevskii, *Electrodynamics of continuous media*, 2nd edition, pp. 279–283, (Butterworth-Heinemann, Oxford, 1984)
13. D. C. Hutchings, M. Sheik-Bahae, D. J. Hagan, and E. W. van Stryland: "Kramers–Krönig relations in nonlinear optics," Opt. Quant. Electron. **24**, 1–30 (1992)
14. M. Beck, I. A. Walmsley, and J. D. Kafka: "Group delay measurements of optical components near 800 nm," IEEE J. Quantum Electron. **27**, 2074–2081 (1991)
15. R. H. J. Kop, P. de Vries, R. Sprik, and A. Lagendijk: "Kramers–Kronig relations for an interferometer," Opt. Commun. **138**, 118–126 (1997)
16. M. A. Muriel and A. Carballar: "Phase reconstruction from reflectivity in uniform fiber Bragg gratings," Opt. Lett. **22**, 93–95 (1997)
17. A. Carballar and M. A. Muriel: "Phase reconstruction from reflectivity in fiber Bragg gratings," J. Lightwave Technol. **15**, 1314–1322 (1997)
18. D. Pastor and J. Capmany: "Experimental demonstration of phase reconstruction from reflectivity in uniform fibre Bragg gratings using the Wiener–Lee transform," Electron. Lett. **34**, 1344–1345 (1998)
19. J. Skaar and H. E. Engan: "Phase reconstruction from reflectivity in fibre Bragg gratings," Opt. Lett. **24**, 136–138 (1999)

20. L. Poladian: "Group-delay reconstruction for fiber Bragg gratings in reflection and transmission," Opt. Lett. **22**, 1571–1573 (1997)
21. F. W. King: "Analysis of optical data by the conjugate Fourier-series approach," J. Opt. Soc. Am. **68**, 994–997 (1978)
22. B. Harbecke: "Application of Fourier's allied integrals to the Kramers–Kronig transformation of reflectance data," Appl. Phys. A **40**, 151–158 (1986)
23. F. W. King: "Efficient numerical approach to the evaluation of Kramers–Kronig transforms," J. Opt. Soc. Am. B **19**, 2427–2436 (2002)
24. K. B. Rochford and S. D. Dyer: "Reconstruction of minimum-phase group delay from fibre Bragg grating transmittance/reflectance measurements," Electron. Lett. **35**, 838–839 (1999)
25. A. Ozcan, M. J. F. Digonnet, and G. S. Kino: "Group delay recovery using iterative processing of amplitude of transmission spectra of fibre Bragg gratings," Electron. Lett. **40**, 1104–1106 (2004)
26. T. Erdogan: "Fiber grating spectra," J. Lightwave Technol. **15**, 1277–1294 (1997)
27. C. J. Brooks, G. L. Vossler, and K. A. Winick: "Phase response measurement technique for waveguide grating filters," Appl. Phys. Lett. **66**, 2168–2170 (1995)
28. S. Barcelos, M. N. Zervas, R. I. Laming, and D. N. Payne; "Interferometric fibre grating characterization," *IEE Colloquium on Optical Fibre Gratings and their Applications*, pp. 5/1–5/7, (1995)
29. S. Barcelos, M. N. Zervas, R. I. Laming, D. N. Payne, L. Reekie, J. A. Tucknott, R. Kashyap, P. F. McKee, F. Sladen, and B. Wojciechowicz: "High accuracy dispersion measurements of chirped fibre gratings," Electron. Lett. **31**, 1280–1282 (1995)
30. M. Beck and I. A. Walmsley: "Measurement of group delay with high temporal and spectral resolution," Opt. Lett. **15**, 492–494 (1990)
31. P. Merritt, R. P. Tatam, and D. A. Jackson: "Interferometric chromatic dispersion measurements on short lengths of monomode optical fiber," J. Lightwave Technol. **7**, 703–716 (1989)
32. X. S. Yao and J. Feinberg: "Simple in-line method to measure the dispersion of an optical system," Appl. Phys. Lett. **62**, 811–813 (1993)
33. D. Müller, J. West, and K. Koch: "Interferometric chromatic dispersion measurement of a photonic bandgap fiber," Proc. SPIE **4870**, 395–403, (2002)
34. P.-L. Francois, M. Monerie, C. Vassallo, Y. Durteste, and F. R. Alard: "Three ways to implement interferencial techniques: application to measurements of chromatic dispersion, birefringence, and nonlinear susceptibilities," J. Lightwave Technol. **7**, 500–513 (1989)
35. K. Naganuma, K. Mogi, and H. Yamada: "Group-delay measurement using the Fourier transform of an interferometric cross correlation generated by white light," Opt. Lett. **15**, 393–395 (1990)
36. S. Diddams and J.-C. Diels: "Dispersion measurements with white-light interferometry," J. Opt. Soc. Am. B **13**, 1120–1129 (1996)
37. J. Gehler and W. Spahn: "Dispersion measurement of arrayed-waveguide gratings by Fourier transform spectroscopy," Electron. Lett. **36**, 338–339 (2000)
38. S. D. Dyer, K. B. Rochford, and A. H. Rose: "Fast and accurate low coherence interferometric measurements of fiber Bragg grating dispersion and reflectance," Opt. Express **5**, 262–266 (1999)

39. M. Volanthen, H. Geiger, M. J. Cole, R. I. Laming, and J. P. Dakin: "Low coherence technique to characterise reflectivity and time delay as a function of wavelength within a long fibre grating," Electron. Lett. **32**, 757–758 (1996)
40. S. D. Dyer and K. B. Rochford: "Low-coherence interferometric measurements of fibre Bragg grating dispersion," Electron. Lett. **35**, 1485–1486 (1999)
41. S. D. Dyer and K. B. Rochford: "Low-coherence interferometric measurements of the dispersion of multiple fiber Bragg gratings," IEEE Photon. Technol. Lett. **13**, 230–232 (2001)
42. H. Yamada, K. Okamoto, A. Kaneko, and A. Sugita: "Dispersion resulting from phase and amplitude errors in arrayed-waveguide grating multiplexers-demultiplexers," Opt. Lett. **25**, 569–571 (2000)
43. H. Yamada, H. Sanjoh, M. Kohtoku, K. Takada, and K. Okamoto: "Measurement of phase and amplitude error distributions in arrayed-waveguide grating multi/demultiplexers based on dispersive waveguide," J. Lightwave Technol. **18**, 1309–1320 (2000)
44. B. Costa, D. Mazzoni, M. Puleo, and E. Vezzoni: "Phase shift technique for the measurement of chromatic dispersion in optical fibers using LED's," IEEE J. Quantum Electron. **QE-18**, 1509–1514 (1982)
45. S. Ryu, Y. Horiuchi, and K. Mochizuki: "Novel chromatic dispersion measurement method over continuous Gigahertz tuning range," J. Lightwave Technol. **7**, 1177–1180 (1989)
46. K. Takiguchi, K. Okamoto, S. Suzuki, and Y. Ohmori: "Planar lightwave circuit optical dispersion equaliser," *Proc. European Conf. Opt. Commun. (ECOC'93)*, vol. 3, pp. 33–36, ThC 12.9 (1993)
47. ITU-T Recommendation G.650.1, *Definition and test methods for linear, deterministic attributes of single-mode fibre and cable* (International Telecommunications Union, Geneva, Switzerland, 2004)
48. T. Niemi, G. Genty, and H. Ludvigsen: "Group-delay measurements using the phase-shift method: improvement on the accuracy," *Proc. European Conf. Opt. Commun. (ECOC'01)*, Amsterdam, The Netherlands, Th.M.1.5 (2001)
49. T. Niemi, M. Uusimaa, and H. Ludvigsen: "Limitations of phase-shift method in measuring dense group delay ripple of fiber Bragg gratings," IEEE Photon. Technol. Lett. **13**, 1334–1336 (2001)
50. W. H. Press, S. A. Teukolsky, W. T. Vetterling, and B. P. Flannery: *Numerical recipes in C*, 2nd edition, Chap. 14.8, (Cambridge University Press, Cambridge, 1992)
51. A. J. Barlow, R. S. Jones, and K. W. Forsyth: "Technique for direct measurement of single-mode fiber chromatic dispersion," J. Lightwave Technol. **LT-5**, 1207–1213 (1987)
52. J. B. Schlager, S. E. Mechels, and D. L. Franzen: "Precise laser-based measurements of zero-dispersion wavelength in single-mode fibers," *Techn. Digest Opt. Fiber Commun. Conf. (OFC'96)*, vol. 2, pp. 293–294, FA2 (1996)
53. S. E. Mechels, J. B. Schlager, and D. L. Franzen: "Accurate measurements of the zero-dispersion wavelength in optical fibers," J. Res. Natl. Inst. Stand. Technol. **102**, 333–347 (1997)
54. G. H. Smith, D. Novak, and Z. Ahmed: "Technique for optical SSB generation to overcome dispersion penalties in fibre-radio systems," Electron. Lett. **33**, 74–75 (1997)

55. J. E. Román, M. Y. Frankel, and R. D. Esman: "Spectral characterization of fiber gratings with high resolution," Opt. Lett. **23**, 939–941 (1998)
56. R. M. Fortenberry: "Enhanced wavelength resolution chromatic dispersion measurements using fixed side-band technique," *Techn. Digest Opt. Fiber Commun. Conf. (OFC'00)*, Baltimore, Maryland, USA, vol 1, pp 107–109, TuG8 (2000)
57. G. Genty, T. Niemi, and H. Ludvigsen: "New method to improve the accuracy of group delay measurements using the phase-shift technique," Opt. Commun. **204**, 119–126 (2002)
58. R. Fortenberry, W. V. Sorin, and P. Hernday: "Improvement of group delay measurement accuracy using a two-frequency modulation phase-shift method," IEEE Photon. Technol. Lett. **15**, 736–738 (2003)
59. T. Dennis and P. A. Williams: "Relative group delay measurements with 0.3 ps resolution: toward 40 Gbit/s component metrology," *Techn. Digest Opt. Fiber Commun. Conf. (OFC'02)*, Anaheim, California, USA, pp 254–256, WK3 (2002)
60. T. Dennis and P. A. Williams: "Chromatic dispersion measurement error caused by source amplified spontaneous emission," IEEE Photon. Technol. Lett. **16**, 2532–2534 (2004)
61. S. Y. Set, M. K. Jablonski, K. Hsu, C. S. Goh, and K. Kikuchi: "Rapid amplitude and group-delay measurement system based on intra-cavity modulated swept-lasers," IEEE Trans. Instrum. Meas. **53**, 192–196 (2004)
62. A. H. Rose, C.-M. Wang, and S. D. Dyer: "Round robin for optical fiber Bragg grating metrology," J. Res. Natl. Inst. Stand. Technol. **105**, 839–866 (2000)
63. F. Devaux, Y. Sorel, and J. F. Kerdiles: "Simple measurement of fiber dispersion and of chirp parameter of intensity modulated light emitter," J. Lightwave Technol. **11**, 1937–1940 (1993)
64. B. Christensen, J. Mark, G. Jacobsen, and E. Bødtker: "Simple dispersion measurement technique with high resolution," Electron. Lett. **29**, 132–134 (1993)
65. C. Peucheret, F. Liu, and R. J. S. Pedersen: "Measurement of small dispersion values in optical components," Electron. Lett. **35**, 409–411 (1999)
66. D. C. Johnson, K. O. Hill, F. Bilodeau, and S. Faucher: "New design concept for a narrowband wavelength-selective optical tap and combiner," Electron. Lett. **23**, 668–669 (1987)
67. C. K. Madsen and J. H. Zhao: *Optical filter design and analysis, a signal processing approach* (Wiley, New York, 1999)
68. M. Scobey and R. Hallock: "Thin film filter based components for optical add/drop," in *OSA Trends in Optics and Photonics*, *WDM components,* (D. A. Nolan, ed.), vol 29, pp. 25–33, (Opt. Soc. America, Washington, DC, 1999)
69. B. Nyman, M. Farries, and C. Si: "Technology trends in dense WDM demultiplexers," Opt. Fib. Technol. **7**, 255–274 (2001)
70. K. Zhang, J. Wang, E. Schwendeman, D. Dawson-Elli, R. Faber, and R. Sharps: "Group delay and chromatic dispersion of thin-film-based, narrow bandpass filters used in dense wavelength-division-multiplexed systems," Appl. Opt **41**, 3172–3175 (2002)
71. R. B.Sargent: "Recent advances in thin film filters," *Techn. Digest Opt. Fiber Commun. Conf. (OFC'04)*, Los Angeles, California, USA, TuD6 (2004)

72. R. M. Fortenberry, M. E.Wescott, L. P. Ghislain, and M. A. Scobey: "Low chromatic dispersion thin film DWDM filters for 40 Gb/s transmission systems," *Techn. Digest Opt. Fiber Commun. Conf. (OFC'02)*, Anaheim, California, USA, pp. 319–320, WS2 (2002)
73. M. Tilsch, C. A. Hulse, F. K. Zernik, R. A. Modavis, C. J. Addiego, R. B. Sargent, N. A. O'Brien, H. Pinkney, and A. V. Turukhin: "Experimental demonstration of thin-film dispersion compensation for 50–GHz filters," IEEE Photon. Technol. Lett. **15**, 66–68 (2003)
74. M. K. Smit and C. van Dam: "PHASAR-based WDM-devices: principles, design and applications," IEEE J. Select. Topics Quantum Electron. **2**, 236–250 (1996)
75. H. Takahashi, K. Oda, H. Toba, and Y. Inoue: "Transmission characteristics of arrayed waveguide N×N wavelength multiplexer," J. Lightwave Technol. **13**, 447–455 (1995)
76. H. Yamada, H. Sanjoh, M. Kohtoku, and K. Takada: "Measurement of phase and amplitude error distributions in InP-based arrayed-waveguide grating multi / demultiplexers," Electron. Lett. **36**, 136–138 (2000)
77. P. Muñoz, D. Pastor, J. Capmany, and S. Sales: "Analytical and numerical analysis of phase and amplitude errors in the performance of arrayed waveguide gratings," IEEE J. Select. Topics Quantum Electron. **8**, 1130–1141 (2002)
78. C. X. Yu, D. T. Neilson, C. R. Doerr, and M. Zirngibl: "Dispersion free (de)mux with record figure-of-merit," IEEE Photon. Technol. Lett. **14**, 1300–1302 (2002)
79. R. Ryf, Y. Su, L. Möller, S. Chandrasekhar, X. Liu, D. T. Neilson, and C. Randy Giles: "Wavelength blocking filter with flexible data rates and channel spacing," J. Lightwave Technol. **23**, 54–61 (2005)
80. O. Schwelb: "Transmission, group delay, and dispersion in single-ring optical resonators and add/drop filters – a tutorial overview," J. Lightwave Technol. **22**, 1380–1394 (2004)
81. X. Liu: "Can 40–Gb/s duobinary signals be carried over transparent DWDM systems with 50–GHz channel spacing," IEEE Photon. Technol. Lett. **17**, 1328–1330, (2005)
82. N. Hanik, A. Ehrhardt, A. Gladisch, C. Peucheret, P. Jeppesen, L. Molle, R. Freund, and C. Caspar: "Extension of all-optical network-transparent domains based on normalized transmission sections," J. Lightwave Technol. **22**, 1439–1453 (2004)
83. A. H. Gnauck and R. M. Jopson: "Dispersion compensation for optical fiber systems," in *Optical Fiber Telecommunications IIIA* (I. P. Kaminow and T. L. Koch, eds.), Chap. 7 (Academic Press, San Diego, 1997)
84. M. Yamada and K. Sakuda: "Analysis of almost-periodic distributed feedback slab waveguides via a fundamental matrix approach," Appl. Opt. **26**, 3474–3478, (1987)
85. M. Ibsen, H. Geiger, and R. I. Laming: "In-band dispersion limitations of uniform apodised fibre gratings," *Proc. European Conf. Opt. Commun. (ECOC'98)*, Madrid, Spain, vol. 1, pp. 413–414 (1998)
86. L. R. Chen and P. W. E. Smith: "Fibre Bragg grating transmission filters with near-ideal filter response," Electron. Lett. **34**, 2048–2050 (1998)
87. G. Nykolak, G. Lenz, B. J. Eggleton, and T. A. Strasser: "Impact of fiber grating dispersion on WDM system performance," *Techn. Digest Opt. Fiber Commun. Conf. (OFC'98)*, San Jose, California, USA, vol. 2, pp. 4–5, TuA3 (1998)

88. G. Nykolak, B. J. Eggleton, G. Lenz, and T. A. Strasser: "Dispersion penalty measurements of narrow fiber Bragg gratings at 10 Gb/s," IEEE Photon. Technol. Lett. **10**, 1319–1321 (1998)
89. G. Lenz, G. Nykolak, and B. J. Eggleton: "Dispersion of optical filters in WDM systems: theory and experiment," *Proc. European Conf. Opt. Commun. (ECOC'98)*, Madrid, Spain, vol. 1, pp. 271–272 (1998)
90. G. Lenz, G. Nykolak, and B. J. Eggleton: "Waveguide grating routers for dispersionless filtering in WDM system at channel rate of 10 Gbit/s," Electron. Lett. **34**, 1683–1684 (1998)
91. P. Leisching, H. Bock, A. Richter, D. Stoll, and G. Fischer: "Optical add/drop multiplexer for dynamic channel routing," Electron. Lett. **35**, 591–592 (1999)
92. K. P. Jones, M. S. Chaudhry, D. Simeonidou, N. H. Taylor, and P. R. Morkel: "Optical wavelength add-drop multiplexer in installed submarine WDM network," Electron. Lett. **31**, 2117–2118 (1995)
93. B. J. Eggleton, G. Lenz, N. Litchinitser, D. B. Patterson, and R. E. Slusher: "Implications of fiber grating dispersion for WDM communication systems," IEEE Photon. Technol. Lett. **9**, 1403–1405 (1997)
94. N. M. Litchinitser, B. J. Eggleton, G. Lenz, and G. P. Agrawal: "Dispersion in cascaded-grating-based add/drop filters," Techn. Dig. Conf. Lasers and Electro-Optics, (CLEO'98), CTh015 (1998)
95. N. M. Litchinitser, B. J. Eggleton, and G. P. Agrawal: "Dispersion of cascaded fiber gratings in WDM lightwave systems," J. Lightwave Technol. **16**, 1523–1529 (1998)
96. H. Geiger and M. Ibsen: "Complexity limitations of optical networks from out-of-band dispersion of grating filters," *Proc. European Conf. Opt. Commun. (ECOC'98)*, Madrid, Spain, vol. 1, pp. 405–406 (1998)
97. L. Poladian: "Design constraints for wavelength-division-multiplexed filters with minimal side-channel impairment," Opt. Lett. **26**, 7–9 (2001)
98. C. Peucheret, A. Buxens, T. Rasmussen, C. F. Pedersen, and P. Jeppesen: "Cascadability of fibre Bragg gratings for narrow channel spacing systems using NRZ and duobinary modulation," *Proc. OptoElectron. Commun. Conf. (OECC'01)*, Sydney, Australia, pp. 92–93, TUA3 (2001)
99. H. Bock, P. Leisching, A. Richter, D. Stoll, and G. Fischer: "System impact of cascaded optical add/drop multiplexers based on tunable fiber Bragg gratings," *Techn. Digest Opt. Fiber Commun. Conf. (OFC'00)*, Baltimore, Maryland, USA, vol. 2, pp. 296–298 (2000)
100. M. Kuznetsov, N. M. Froberg, S. R. Henion, C. Reinke, and C. Fennelly: "Dispersion-induced power penalty in fiber-Bragg-grating WDM filter cascades using optically preamplifed and nonpreamplified receivers," IEEE Photon. Technol. Lett. **12**, 1406–1408 (2000)
101. M. Kuznetsov, N. M. Froberg, S. R. Henion, C. Reinke, C. Fennelly, and K. A. Rauschenbach: "Dispersion-induced power penalty in fiber-Bragg-grating WDM filter cascades," *Techn. Digest Opt. Fiber Commun. Conf. (OFC'00)*, Baltimore, Maryland, vol. 2, pp. 311–313 (2000)
102. K. H. Ylä-Jarkko, M. N. Zervas, M. K. Durkin, I. Barry, and A. B. Grudinin: "Power penalties due to in-band and out-of-band dispersion in FBG cascades," J. Lightwave Technol. **21**, 506–510 (2003)

103. S. Bigo: "Multiterabit/s DWDM terrestrial transmission with bandwidth-limiting optical filtering," IEEE J. Select. Topics Quantum Electron. **10**, 329–340 (2004)
104. H. Kim and A. H. Gnauck: "10 Gbit/s 177 km transmission over conventional singlemode fibre using a vestigial side-band modulation format," Electron. Lett. **37**, 1533–1534 (2001)
105. Y. Kim, S. Kim, I. Lee, and J. Jeong: "Optimization of transmission performance of 10–Gb/s optical vestigial side-band signals using electrical dispersion compensation by numerical simulation," IEEE J. Select. Topics Quantum Electron. **10**, 371–375 (2004)
106. C. X. Yu, S. Chandrasekhar, T. Zhou, and D. T. Neilson: "0.8 bit/s/Hz spectral efficiency at 10 Gbit/s via vestigial-side-band filtering," Electron. Lett. **39**, 225–227 (2003)
107. K. Ennser, M. N. Zervas, and R. I. Laming: "Optimization of apodized linearly chirped fiber gratings for optical communications," IEEE J. Quantum Electron. **34**, 770–778 (1998)
108. H. Chotard, Y. Painchaud, A. Mailloux, M. Morin, F. Trépanier, and M. Guy: "Group delay ripple of cascaded Bragg grating gain flattening filters," IEEE Photon. Technol. Lett. **14**, 1130–1132 (2002)
109. D. B. Stegall and T. Erdogan: "Dispersion control with use of long-period fiber gratings," J. Opt. Soc. Am. A **17**, 304–312 (2000)
110. C. K. Madsen, G. Lenz, A. J. Bruce, M. A. Cappuzzo, L. T. Gomez, and R. E. Scotti: "Integrated all-pass filters for tunable dispersion and dispersion slope compensation," IEEE Photon. Technol. Lett. **11**, 1623–1625 (1999)
111. C. K. Madsen: "Subband all-pass filter architectures with applications to dispersion and dispersion-slope compensation and continuously variable delay lines," J. Lightwave Technol. **21**, 2412–2420 (2003)
112. L. Poladian: "Graphical and WKB analysis of nonuniform Bragg gratings," Phys. Rev. E **48**, 4758–4767 (1993)
113. L. Poladian: "Understanding profile-induced group-delay ripple in Bragg gratings," Appl. Opt. **39**, 1920–1923 (2000)
114. M. Sumetsky, B. J. Eggleton, and C. Martijn de Sterke: "Theory of group delay ripple generated by chirped fiber gratings," Opt. Express **10**, 332–340, 2002
115. R. L. Lachance, M. Morin, and Y. Painchaud: "Group delay ripple in fibre Bragg grating tunable dispersion compensators," Electron. Lett. **38**, 1505–1507 (2002)
116. M. Sumetsky, P. I. Reyes, P. S. Westbrook, N. M. Litchinitser, B. J. Eggleton, Y. Li, R. Deshmukh, and C. Soccolich: "Group-delay ripple correction in chirped fiber Bragg gratings," Opt. Lett. **28**, 777–779 (2003)
117. S. G. Evangelides Jr., N. S. Bergano, and C. R. Davidson: "Intersymbol interference induced by delay ripple in fiber Bragg gratings," *Techn. Digest Opt. Fiber Commun. Conf. (OFC'99)*, San Diego, California, USA, vol. 4, pp. 5–7, FA2 (1999)
118. T. N. Nielsen, B. J. Eggleton, and T. A. Strasser: "Penalties associated with group delay imperfections for NRZ, RZ and duo-binary encoded optical signals," *Proc. European Conf. Opt. Commun. (ECOC'99)*, Nice, France, vol. 1, pp. 388–389 (1999)
119. C. Scheerer, C. Glingener, G. Fischer, M. Bohn, and W. Rosenkranz: "Influence of filter group delay ripples on system performance," *Proc. European Conf. Opt. Commun. (ECOC'99)*, Nice, France, vol. 1, pp. 410–411 (1999)

120. C. Riziotis and M. N. Zervas: "Effect of in-band group delay ripple on WDM filter performance," *Proc. European Conf. Opt. Commun. (ECOC'01)*, Amsterdam, The Netherlands, vol. 4, pp. 492–493, Th.M.1.3 (2001)
121. K. Hinton: "Metrics for dispersion ripple in optical systems," Opt. Fib. Technol. **10**, 50–72 (2004)
122. K. Ennser, M. Ibsen, M. Durkin, M. N. Zervas, and R. I. Laming: "Influence of nonideal chirped fiber grating characteristics on dispersion cancellation," IEEE Photon. Technol. Lett. **10**, 1476–1478 (1998)
123. D. Penninckx, S. Khalfallah, and P. Brosson: "System impact of phase ripples in optical components," *Techn. Digest Opt. Fiber Commun. Conf. (OFC'01)*, Anaheim, California, USA, ThB4 (2001)
124. X. Liu, L. F. Mollenauer, and X. Wei: "Impact of group-delay ripple in transmission systems including phase-modulated formats," IEEE Photon. Technol. Lett. **16**, 305–307 (2004)
125. H. Yoshimi, Y. Takushima, and K. Kikuchi, "A simple method for estimating the eye-opening penalty caused by group-delay ripple of optical filters," *Proc. European Conf. Opt. Commun. (ECOC'02)*, Copenhagen, Denmark, vol. 4, 10.4.4 (2002)
126. N. Cheng, D. J. Krause, and J. C. Cartledge: "Measuring frequency response of dispersion compensating fibre Bragg grating using Fourier coefficients," Electron. Lett. **41**, 402–403 (2005)
127. M. H. Eiselt, C. B. Clausen, and R. W. Tkach: "Performance characterization of components with group delay fluctuations," IEEE Photon. Technol. Lett. **15**, 1076–1078 (2003)
128. B. J. Eggleton, A. Ahuja, P. S. Westbrook, J. A. Rogers, P. Kuo, T. N. Nielsen, and B. Mikkelsen: "Integrated tunable fiber gratings for dispersion management in high-bit rate systems," J. Lightwave Technol. **18**, 1418–1432 (2000)
129. B. J. Eggleton, A. Ahuja, P. S. Westbrook, J. A. Rogers, P. Kuo, T. N. Nielsen, and B. Mikkelsen: "Correction to : Integrated tunable fiber gratings for dispersion management in high-bit rate systems," J. Lightwave Technol. **18**, 1591 (2000)
130. S. Jamal and J. C. Cartledge: "Variation in the performance of multispan 10–Gb/s systems due to the group delay ripple of dispersion compensating fiber Bragg gratings," J. Lightwave Technol. **20**, 28–35 (2002)
131. V. Mizrahi and J. E. Sipe: "Optical properties of photosensitive fiber phase gratings," J. Lightwave Technol. **11**, 1513–1517 (1993)
132. E. Delevaque, S. Boj, J.-F. Bayon, H. Poignant, J. Le Mellot, M. Monerie, P. Niay, and P. Bernage: "Optical fiber design for strong gratings photoimprinting with radiation mode suppression," *Techn. Digest Opt. Fiber Commun. Conf. (OFC'95)* PD5 (1995)
133. F. Bakhti, F. Bruyère, X. Daxhelet, X. Shou, J. Da Loura, S. Lacroix, and P. Sansonetti: "Grating-assisted Mach–Zehnder OADM using photosensitive-cladding fibre for cladding mode coupling reduction," Electron. Lett. **35**, 1013–1014 (1999)
134. K. Okamoto and H. Yamada: "Arrayed-waveguide grating multiplexer with flat spectral response," Opt. Lett. **20**, 43–35 (1995)

135. Y. P. Ho, H. Li, and Y. J. Chen: "Flat channel-passband-wavelength multiplexing and demultiplexing devices by multiple-Rowland-circle design," IEEE Photon. Technol. Lett. **9**, 342–344 (1997)
136. C. Dragone, T. Strasser, G. A. Bogert, L. W. Stulz, and P. Chou: "Waveguide grating router with maximally flat passband produced by spatial filtering," Electron. Lett. **33**, 1312–1314 (1997)
137. A. Rigny, A. Bruno, and H. Sik: "Multigrating method for flattened spectral response wavelength multi/demultiplexer," Electron. Lett. **33**, 1701–1702 (1997)
138. C. Dragone: "Efficient techniques for widening the passband of a wavelength router," J. Lightwave Technol. **16**, 1895–1906 (1998)
139. L. B. Soldano and E. C. M. Pennings: "Optical multi-mode interference devices based on self-imaging: principles and applications," J. Lightwave Technol. **13**, 615–627 (1995)
140. J. B. D. Soole, M. R. Amersfoort, H. P. LeBlanc, N. C. Andreadakis, A. Rajhel, C. Caneau, R. Bhat, M. A. Koza, C. Youtsey, and I. Adesida: "Use of multimode interference couplers to broaden the passband of wavelength-dispersive integrated WDM filters," IEEE Photon. Technol. Lett. **8**, 1340–1342 (1996)
141. M. R. Amersfoort, J. B. D. Soole, H. P. LeBlanc, N. C. Andreadakis, A. Rajhel, and C. Caneau: "Passband broadening of integrated arrayed waveguide filters using multimode interference couplers," Electron. Lett. **32**, 449–451 (1996)
142. K. Okamoto and A. Sugita: "Flat spectral response arrayed-waveguide grating multiplexer with parabolic waveguide horns," Electron. Lett. **32**, 1661–1662 (1996)
143. M. E. Marhic and X. Yi: "Calculation of dispersion in arrayed waveguide grating demultiplexers by a shifting-image method," IEEE J. Select. Topics Quantum Electron. **8**, 1149–1157 (2002)
144. T. Kitoh, Y. Inoue, M. Itoh, M. Kotoku, and Y. Hibino: "Low chromatic-dispersion flat-top arrayed waveguide grating filter," Electron. Lett. **39**, 1116–1118 (2003)
145. B. Fondeur, A. L. Sala, H. Yamada, R. Brainard, E. Egan, S. Thedki, N. Gopinathan, D. Nakamoto, and A. Vaidyanathan: "Ultrawide AWG with hyper-Gaussian profile," IEEE Photon. Technol. Lett. **16**, 2628–2630, (2004)
146. H. Kogelnik: "Filter response of nonuniform almost-periodic structures," Bell Syst. Techn. J. **55**, 109–126 (1976)
147. G. Hugh Song: "Theory of symmetry in optical filter responses," J. Opt. Soc. Am. A. **11**, 2027–2037 (1994)
148. M. Ibsen, M. K. Durkin, M. J. Cole, and R. I. Laming: "Optimised square passband fibre Bragg grating filter with in-band flat group delay response," Electron. Lett. **34**, 800–802 (1998)
149. T. Shibata, M. Shiozaki, M. Ohmura, K. Murashima, A. Inoue, and H. Suganuma: "The dispersion-free filters for DWDM systems using 30 mm long symmetric fiber Bragg gratings," *Techn. Digest Opt. Fiber Commun. Conf. (OFC'01)*, Anaheim, California, USA, WDD84 (2001)
150. T. Shibata, K. Murashima, K. Hashimoto, M. Shiozaki, T. Iwashima, T. Okuno, A. Inoue, and H. Suganuma: "The novel dispersion reduced fiber Bragg grating suitable for 10 Gb/s DWDM systems," IEICE Trans. Electron. **E85-C**, 927–933, (2002)

151. M. Ibsen, R. Feced, P. Petropoulos, and M. N. Zervas: "99.9% reflectivity dispersion-less square-filter fibre Bragg gratings for high speed DWDM networks," *Techn. Digest Opt. Fiber Commun. Conf. (OFC'00)*, Baltimore, Maryland, USA, PD21 (2000)
152. M. Ibsen, R. Feced, P. Petropoulos, and M. N. Zervas: "High reflectivity linear-phase fibre Bragg gratings," *Proc. European Conf. Opt. Commun. (ECOC'00)*, Munich, Germany, vol. 1, pp. 53–54 (2000)
153. M. Ibsen, P. Petropoulos, M. N. Zervas, and R. Feced: "Dispersion-free fibre Bragg gratings," *Techn. Digest Opt. Fiber Commun. Conf. (OFC'01)*, San Diego, California, USA, MC1 (2001)
154. M. Ibsen, R. Feced, J. A. J. Fells, and W. S. Lee: "40 Gbit/s high performance filtering for DWDM networks employing dispersion-free fibre Bragg gratings," *Proc. European Conf. Opt. Commun. (ECOC'01)*, Amsterdam, The Netherlands, vol. 4, pp. 594–595, Th.B.2.1 (2001)
155. R. Feced, M. N. Zervas, and M. A. Muriel: "An efficient inverse scattering algorithm for the design of nonuniform fiber Bragg gratings," IEEE J. Quantum Electron. **35**, 1105–1115 (1999)
156. M. Ibsen and R. Feced: "Fiber Bragg gratings for pure dispersion-slope compensation," Opt. Lett. **28**, 980–982 (2003)
157. H.-J. Deyerl, C. Peucheret, B. Zsigri, F. Floreani, N. Plougmann, S. J. Hewlett, M. Kristensen, and P. Jeppesen: "A compact low dispersion fiber Bragg grating with high detuning tolerance for advanced modulation formats," Opt. Commun. **247**, 93–100 (2005)
158. H. J. Deyerl, N. Plougmann, J. B. Jensen, F. Floreani, H. R. Sørensen, and M. Kristensen: "Fabrication of advanced Bragg gratings with complex apodization profiles by use of the polarization control method," Appl. Opt. **43**, 3513–3522 (2004)